Elsevier Editorial System(tm) for Mechanical Systems and Signal Processing

Manuscript Draft

Manuscript Number: MSSP17-1553R1

Title: Rolling Mass Energy Harvester for Very Low Frequency of Input Vibrations

Article Type: SI:Explore NL Benefits

Keywords: energy harvesting; Tusi couple; nonlinear systems; human motion; low frequency; electromagnetic induction

Corresponding Author: Mr. Jan Smilek,

Corresponding Author's Institution: Brno University of Technology

First Author: Jan Smilek

Order of Authors: Jan Smilek; Zdenek Hadas; Jan Vetiska; Steve Beeby

Rolling Mass Energy Harvester for Very Low Frequency of Input Vibrations

Jan Smilek[a,*], Zdenek Hadas[a], Jan Vetiska[a], Steve Beeby[b]

[a] Faculty of Mechanical Engineering, Brno University of Technology, Technicka 2896/2, 616 69 Brno, Czech Republic
[b] School of Electronics and Computer Science, University of Southampton, Highfield, Southampton, Hampshire, SO17 1BJ, United Kingdom
[*] E-mail: smilek@fme.vutbr.cz

Abstract – This paper presents a novel design of a nonlinear kinetic energy harvester for very low excitation frequencies below 10 Hz. The design is based on a proof mass, rolling in a circular cavity in a Tusi couple configuration. This allows for an unconstrained displacement of the proof mass while maintaining the option of keeping the energy transduction element engaged during the whole cycle and thus reducing the required number of transduction elements. Both the presented model and the fabricated prototype of the device employ electromagnetic induction to harvest energy from low frequency and low magnitude vibrations that are typically associated with human movements. The prototype demonstrated an average power of 5.1 mW from a 1.3 g periodic acceleration waveform at 2.78 Hz. The highest simulated normalized power density reaches up to 230 $\mu W/g^2/cm^3$, but this depends heavily on the excitation conditions.

Keywords- energy harvesting; Tusi couple; nonlinear systems; human motion; low frequency; electromagnetic induction

1. Introduction

Powering up mostly small electronic devices by the means of independent power sources based on energy harvesting principle has attracted a growing interest in recent years. Instead of utilizing traditional primary or secondary battery cells, or using wiring to supply power directly from the grid or a central power source, there is considerable interest in the exploitation of otherwise wasted energy present in the ambient environment of the electronic device. Such energy harvesting approaches enable compact and standalone wireless system nodes, reducing the cost and weight associated with wiring, and the maintenance costs of periodic battery replacement.

Depending on the intended application, the available ambient energy sources might include solar, temperature gradient, fluid flow, pressure variations or kinetic energy. As the amount of ambient energy is usually limited and the size of the energy harvester is constrained, harvesters are being developed mainly for low-power power devices, such as wireless sensor nodes for structural health monitoring [1] in aerospace or industrial environments [2]. With the increasing prevalence of smart electronics for everyday use another widely considered application field is wearable sensors, electronic gadgets, and biomedical implants [3], [4].

Ambient energy in the environment of the human body is sometimes captured by the use of thermoelectric generators [5], [6] or photovoltaic panels [7], the most common approach lies in exploiting the mechanical energy from human activity. Some locations on the human body allow for utilizing direct force excitation and associated deformation [8]. Examples of direct force harvesters include the deformation of shoe soles [9], the bending of the knee whilst walking [10] and even the deformation of the ear canal when talking or chewing [11]. Some publications also investigate harvesting the energy from the pulsation of arterial vessels or the heart [12].

Another option is to utilize an inertial oscillation mechanism excited by mechanical displacements during human activity. This is the preferred approach in locations where direct forces cannot be exploited, such as at the forearm or hip [13].

Inertial harvesting mechanisms are commonly used in energy harvesters for industrial applications where numerous linear and nonlinear structures have been demonstrated [14], [15]. In the environment of the human body, however, this approach bears considerable additional challenges. For example, the characteristics of the human motion differ significantly between different locations on the body, different types of activity and, for a given location and activity, even between different people [16], [17]. In addition, both the frequency and magnitude commonly associated with human activities are very low [18], [19], and therefore the inertial harvester design becomes quite heavy and bulky in order to satisfy the application power requirements.

However, with the ever decreasing power consumption and increasing efficiency of power-management circuits in modern wearable and biomedical electronic applications, the size of the energy harvesters to power them up is also shrinking down, with some of the designs being small enough to actually present a feasible power source solution [20].

Common methods of transducing the kinetic energy of the vibrating inertial proof mass into electricity include piezoelectric effect, electrostatic conversion, electromagnetic induction, and lately also the triboelectric effect. Piezoelectric transducers are the most commonly used mechanism for harvesting human energy [21]–[23], regardless of their rather high impedance. Electrostatic harvesters [24], [25] are popular due to their compatibility with MEMS fabrication processes, but their need for a priming voltage drags reduces their practicality. Triboelectric harvesters are gaining popularity in last few years, with potential applications including human power [26]. Electromagnetic transducers are quite common in larger scale industrial applications, but scaling these down in size to make them suitable for human power harvesting presents a technical challenge due to reducing the electromechanical coupling coefficient [27]. Complex energy harvesting approaches, such as nonlinear system design [28], frequency up-conversion [29], or parametric resonators [30] are being employed in order to improve the performance of the energy harvesters in certain applications. Various designs of human powered inertial energy harvesters have been demonstrated including linear trajectory oscillation structures (either suspended [31] or free moving with the displacement limited by the use of mechanical bumpers[32], [33]), cantilevers with nonlinear frequency response, arrays of independent oscillators or rotational harvesters [34], frequency up-conversion mechanisms and chaotic motion harvesters [35].

However, the excitation by human power is considered unpredictable [36] and only a small fraction of all the kinetic energy harvester designs introduced in the last two decades [37]–[39] are capable of working in the excitation frequency range below 10 Hz. In this paper we introduce a novel design of nonlinear energy harvester based on a Tusi couple configuration designed for very low excitation frequency in the range between 2 and 10 Hz.

2. Novel Mechanism for Energy Harvesting from Low Frequency Vibrations

The downside of most mechanisms suitable for low frequency excitation is that they are either large in size in order to accommodate the high amplitude proof mass displacements, or they employ mechanical limiters, leading to additional mechanical energy losses and physical wear of components. Pendulum harvesters can theoretically have unlimited displacement, as the pendulum can rotate around its pivotal point. Implementing the transduction mechanism in the pendulum structures with large displacements is challenging and they will either employ multiple transduction elements (e.g. pickup coils in electrodynamic harvester) along the path of the proof mass [40], or increase their total weight by using a proof mass only as a mechanical energy storage element, which is mechanically linked to a separate energy transducing mechanism [41].

The Tusi couple configuration enables unlimited displacements and can be designed in such a way, that a single transduction element can be used irrespective of the inertial mass position. This allows for reduced cost and complexity of the power management electronics whilst slightly increasing the precision required in the mechanical design compared to most common energy harvesting devices.

The proposed mechanism consists of a cylindrical proof mass placed inside a circular cavity in such a way, that only a rolling motion of the proof mass along the cavity wall is possible. During the motion every point on the diameter of the proof mass travels along hypocycloidal path. This can be described using a Cartesian coordinate system, the origin of which lies in the centre of the circular cavity with radius R. The initial position of the proof mass is in the bottom of the cavity.

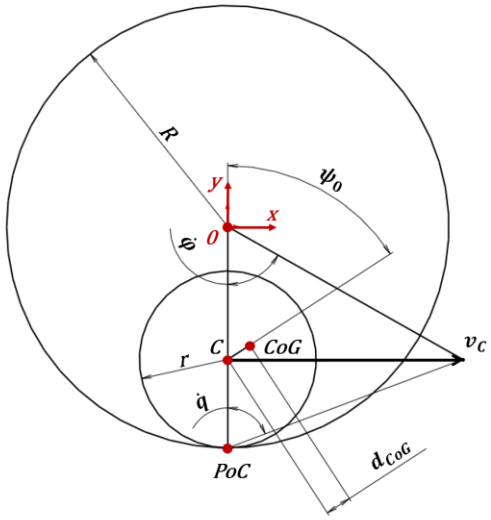

***Fig. 1** Rolling mass harvester geometry*

The position of the centre of the rolling mass C as a function of the angle between the cavity centre and the proof mass centre φ (Fig. 1) is then defined by a set of parametric equations:

$$x_C = (R - r)\sin(\varphi) \tag{1}$$

$$y_C = -(R - r)\cos(\varphi) \tag{2}$$

Constants R and r are the radiuses of the cavity and the proof mass, respectively. The position of the point on the rolling mass that is initially in contact with the circular cavity and that moves along the hypocycloidal path (blended with the PoC in the figure) can be determined from:

$$x_{hypo} = x_C - r \cdot \sin\left(\frac{R - r}{r}\varphi\right) \tag{3}$$

$$y_{hypo} = y_C - r \cdot \cos\left(\frac{R - r}{r}\varphi\right) \tag{4}$$

In case of the centre of gravity CoG not being in the geometric centre of the rolling mass C, its position during the proof motion mass follows a hypotrochoid, and is given by a set of equations:

$$x_{CoG} = x_C + d_{CoG} \cdot \sin\left(\frac{R - r}{r}\varphi + \psi_0\right) \tag{5}$$

$$y_{CoG} = y_C + d_{CoG} \cdot \cos\left(\frac{R - r}{r}\varphi + \psi_0\right) \tag{6}$$

Where d_{CoG} is the distance of the proof mass centre of gravity from the geometrical centre, and ψ_0 is the initial angle between the vertical and the connector of C with CoG. The position of the instantaneous point of contact PoC between the rolling mass and the cavity is found from:

$$x_{PoC} = R\sin(\varphi) \tag{7}$$

$$y_{PoC} = -R\cos(\varphi) \tag{8}$$

The Tusi couple is a special case of this setup, where the ratio of the cavity radius to the rolling mass radius is 2:1. In this case the hypocycloids created by the points on the outer diameter of the rolling mass blend with the straight lines noting the diameter of the cavity (Fig. 2).

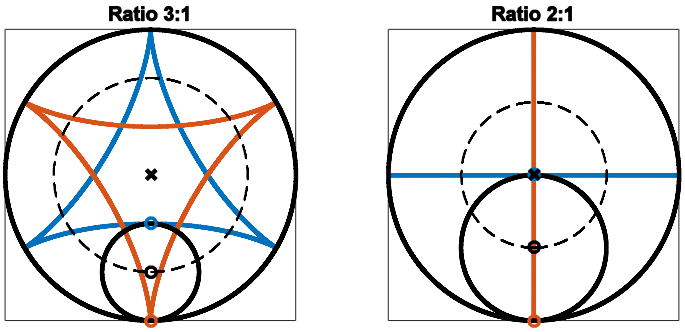

Fig. 2 Comparison of hypocycloidal paths of points on the proof mass for different ratios of cavity to proof mass diameter

Every point on the diameter of the rolling mass travels through the centre of the cavity twice during each revolution cycle. A point of the proof mass currently aligned with the centre of the cavity also has the largest instantaneous velocity in the mechanism, making this location advantageous for velocity damper type energy transduction element placement (Fig. 3).

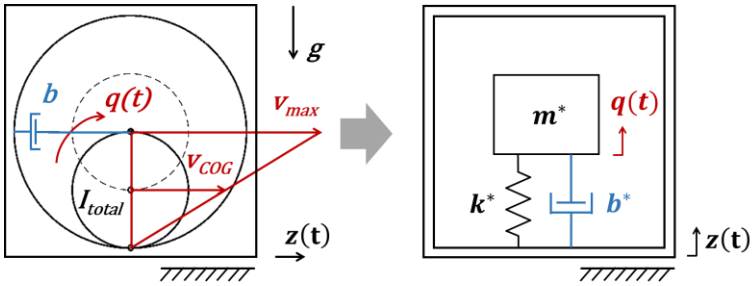

Fig. 3 Tusi couple as spring mass damper system with 1 DoF

Since the movement of the proof mass is constrained in such a way that the rolling motion is ensured, the whole system has only one remaining degree of freedom and can be treated as such. Its dynamics under base excitation is described by the Lagrange's equation of the second kind

$$\frac{d}{dt}\left(\frac{dE_k}{d\dot{q}}\right) - \frac{dE_k}{dq} + \frac{dE_b}{d\dot{q}} + \frac{dE_p}{dq} = -\frac{dA}{dq} = -Q \tag{9}$$

The generalized coordinate q in this case denotes the angular position of the proof mass, which is a function of the angle φ:

$$q = \frac{R-r}{r}\varphi \tag{10}$$

Time derivatives of the generalized coordinate q are denoted with dots above the variable. The rolling movement of the proof mass can be understood as a rotation around a variable axis, which passes through the instantaneous point of contact between the proof mass and the frame, perpendicular to the plane of movement. Employing the parallel axis theorem the kinetic energy of such a movement is:

$$E_k = \frac{1}{2} I_{total}\dot{q}^2 = \frac{1}{2}(I_{CoG} + m \cdot {d_{PoC-CoG}}^2)\dot{q}^2 \tag{11}$$

Where I_{CoG} denotes the moment of inertia of the proof mass with respect to its centre of gravity, m is the weight of the proof mass and $d_{PoC-CoG}$ is the distance between the instantaneous point of contact and the proof mass centre of gravity. Depending on the mass distribution within the rolling element, the distance between the point of contact PoC and the centre of gravity CoG is generally a function of the instantaneous position q:

$$d_{CoG-PoC} = \sqrt{(x_{CoG-PoC})^2 + (y_{CoG-PoC})^2} \tag{12}$$

$$x_{CoG-PoC} = (x_{CoG} - x_{PoC}) \tag{13}$$

$$y_{CoG-PoC} = (y_{CoG} - y_{PoC}) \tag{14}$$

In the special case where the centre of gravity is aligned with the centre of the rolling mass, the distance $d_{PoC-CoG}$ is constant:

$$d_{CoG-PoC_{centre}} = r \tag{15}$$

It is clear that in the general case the $d_{CoG-PoC}$ is a function of instantaneous position. Therefore the derivative of the kinetic energy with respect to position $\frac{dE_k}{dq}$ has generally a nonzero value, which needs to be taken into account when modelling the general mechanism.

The potential energy of the system depends on the global orientation of the mechanism, as there are no additional spring elements employed. In the intended orientation, where the proof mass moves in the vertical plane, the potential energy depends on the height of its centre of gravity, and can be written as:

$$E_p = mgh_{COG} \tag{16}$$

The instantaneous height can then be found as:

$$h_{COG} = y_{CoG}(\varphi) - y_{CoG}(\varphi = 0) \tag{17}$$

In the special case of the centre of gravity being in the centre of the rolling mass ($d_{CoG} = 0$), the equation (17) can be written as

$$h_{COG_{centre}} = (R - r)[1 - \cos(\varphi)] = (R - r)\left[1 - \cos\left(\frac{r}{R - r}q\right)\right] \tag{18}$$

The mechanical energy of the energy harvester is being dissipated from the system in a form of unavoidable mechanical losses and as an electric energy, part of which is dissipated on the impedance of the transduction mechanism, and other part is being delivered to the electric load. The dissipation energy of this system is thus found as a function of mechanical damping b_m^* and electrical damping b_e^*:

$$E_d = \frac{1}{2}b^*\dot{q}^2 = \frac{1}{2}(b_m^* + b_e^*)\dot{q}^2 \tag{19}$$

The mechanical damping b_m^* is affected significantly by the choice of material, and by the manufacturing and assembly precision. These losses are summarized in the mechanical quality factor Q_m.

$$b_m^* = \frac{I_{total} \cdot \Omega}{Q_m} \tag{20}$$

Where Ω is the natural frequency of the mechanism, which can be calculated in the same manner as for a pendulum, assuming small displacements and taking into account the distance between the pivot point and the centre of gravity:

$$\Omega = \sqrt{\frac{k^*}{m^*}} = \sqrt{\frac{mgd_{CoG-PoC}}{I_{total}}} \tag{21}$$

The electrical damping b_e^* is directly proportional to the squared electromechanical coupling coefficient c and indirectly proportional to the total impedance loading Z_{total}:

$$b_e^* = \frac{c^2}{Z_{total}} \tag{22}$$

In case of using the electromagnetic transducer the coupling coefficient is found as

$$c = \frac{d\phi}{dq} \tag{23}$$

Where ϕ is total magnetic flux through the coil. The total impedance is a sum of the load impedance Z_L and the transducer inner impedance Z_C.

$$Z_{total} = Z_L + Z_C \tag{24}$$

The inductance of the coreless pickup coil can be neglected, and the assuming the load impedance is resistive, the equation (22) can therefore be written as:

$$b_e^* = \frac{\left(\frac{d\phi}{dq}\right)^2}{R_L + R_C} \tag{25}$$

The excitation of the system Q is caused by the input acceleration, creating a torque acting upon the rolling proof mass:

$$Q = m\left(\ddot{z}_x \cdot y_{CoG-PoC} + \ddot{z}_y \cdot x_{CoG-PoC}\right) \tag{26}$$

Where $\ddot{z}_x$ and $\ddot{z}_y$ are accelerations of the frame in x and y directions, respectively. In this design study, where the centre of gravity is aligned with the centre of the rolling element, the final form of the equation of motion (5) obtained by combining equations (9)-(26) takes the form:

$$I_{total}\ddot{q} - 0 + (b_e^* + b_m^*)\dot{q} + mgr \cdot \sin\left(\frac{r}{R-r}q\right) = -mr\left(\ddot{z}_x \cdot cos(\frac{r}{R-r}q) + \ddot{z}_y \cdot sin(\frac{r}{R-r}q)\right) \quad (27)$$

This equation is implemented in the simulation model to predict and evaluate the performance of the harvester in different scenarios.

3. Harvester Design and Modelling

Model based design [42] was employed using CAD and FEM software tools together with the derived analytical model to sketch, evaluate and improve the mechanism in terms of the generated power output. Multiple design iteration cycles resulted in a variant with 12 permanent magnets arranged in two groups of six, one group on each face of the rolling proof mass (Fig. 4).

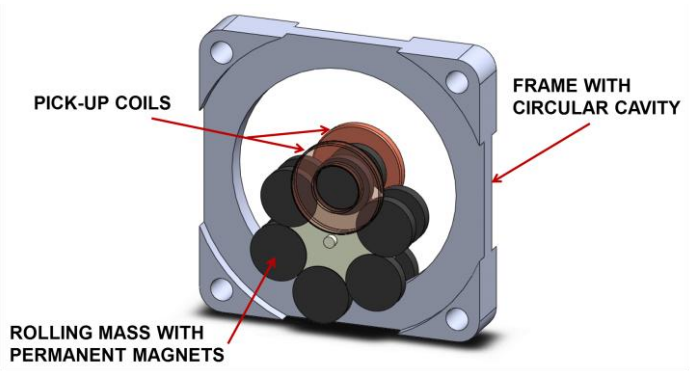

Fig. 4 *Design of the energy harvester based on Tusi couple*

The magnetization direction of each two neighbouring magnets is alternated to maximize the electromechanical coupling coefficient (Fig. 5). Material properties and magnetic field parameters through the coil volume were analysed in CAD and FEM software and used as design parameters in the simulation model.

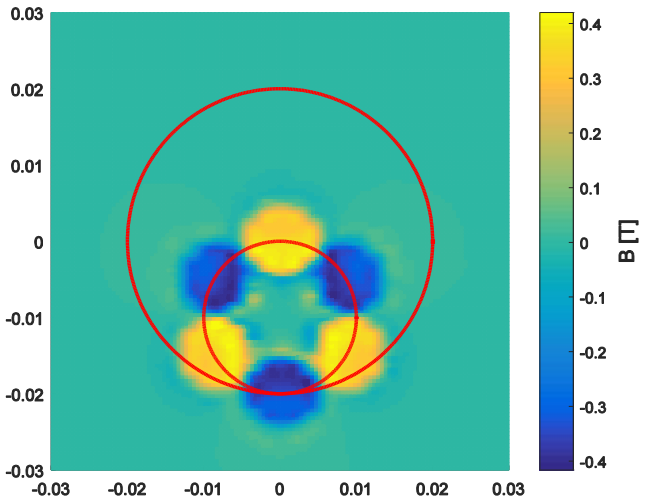

Fig. 5 *Magnetic field distribution 0.5 mm above the magnets surface in the default mechanism position. Cavity and rolling mass diameters in red.*

Analysis of the magnetic field distribution (Fig. 6), and its rate of change in the proximity of the cavity face for different displacement angles (Fig. 7) illustrates the optimum coil position above the centre of the circular cavity, as close as possible to the magnet surface plane. The magnets used both in simulations and in fabricated prototype are made of neodymium, iron and boron alloy $Nd_2Fe_{14}B$.

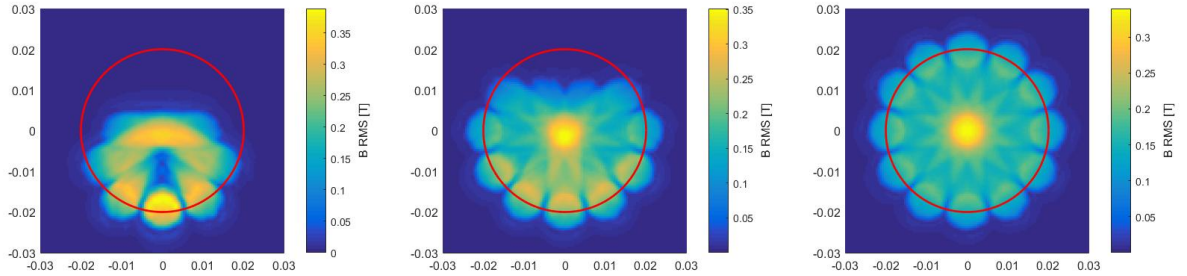

*Fig. 6 Effective magnetic **flux density** 0.5 mm above the magnets surface during a simulated motion of the mechanism with constant speed in limit displacement angles $\pm\frac{\pi}{6}$ (left), $\pm\frac{\pi}{2}$ (middle), and $\pm\pi$ (right). Cavity diameter in red.*

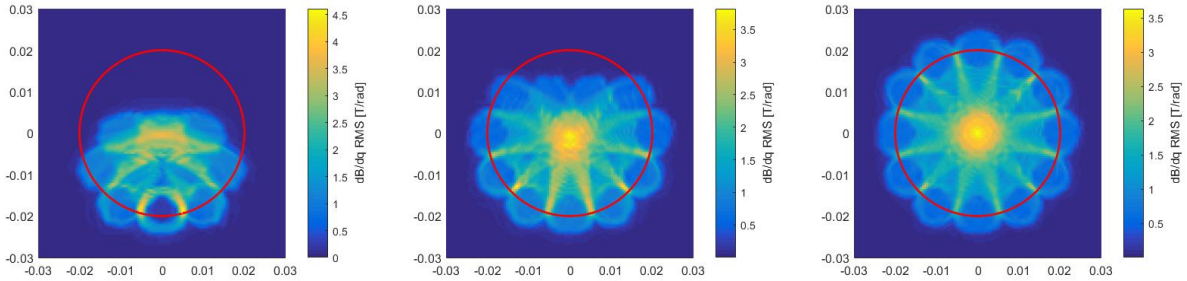

*Fig. 7 Effective magnetic **flux density rate of change** in the cavity area 0.5 mm above the magnets surface during the mechanism motion. Limit displacement angles $\pm\frac{\pi}{6}$ (left), $\pm\frac{\pi}{2}$ (middle), and $\pm\pi$ (right). Cavity diameter in red.*

The pair of coils is located at the optimum position on either side sides of the cavity above its centre. A realistic magnetic circuit model can then be developed, taking into account the thickness of the coil wire, the coil fill factor and the number of turns used. The magnetic flux through each of the coil turns is calculated separately and summed to give the total magnetic flux through the coil. This approach prevents the magnetic circuit model from overestimating the induced voltage due to incorrectly estimated magnetic flux change ratio.

The calculated total magnetic flux through the designed coil volume dependency on the proof mass position follows a sinusoidal waveform (Fig. 8). Knowing the magnetic flux change ratio through the volume of space occupied by the coil also allows for future optimization of coil parameters in order to maximize the power output delivered to the electric load.

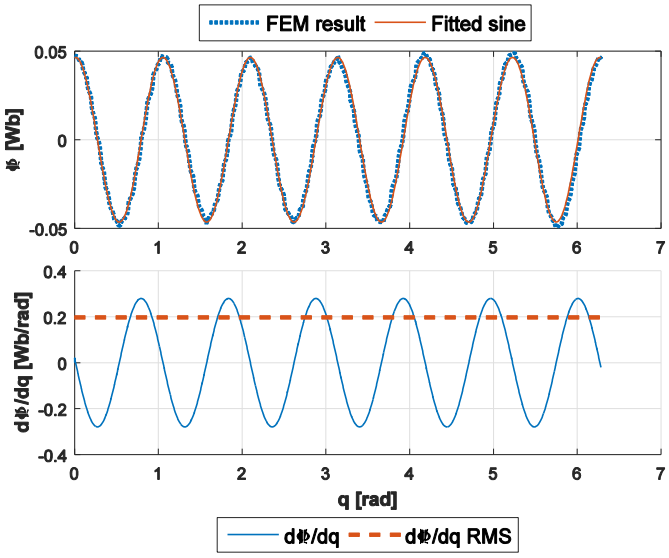

Fig. 8 Total magnetic flux through the coil and its rate of change as a function of proof mass position

4. Prototype fabrication

A prototype of the harvester (Fig. 9) was manufactured using conventional manufacturing methods. The frame of the harvester was manufactured from non-magnetic and electrically non-conductive materials to prevent the induction of eddy currents in the frame and related energy losses. The pair of cylindrical coreless coils was wound manually using insulated copper wire of 50µm diameter. The contact surfaces of the proof mass and the frame were roughened to promote the rolling motion without sliding. The leading slots for the pegs that prevent a free movement of the proof mass inside the cavity are milled into covering lids made of low friction plastic material PE 1000 to minimize mechanical losses in the mechanism. The measured and estimated parameters of the harvester prototype are summarized in Tab. 1. In order to enable reliable manufacture, the initial harvester design was scaled up in size by a factor of 2.

Parameter	**Value**	**Unit**
Total dimensions	50x50x20	mm
Total weight	56.3	g
Frame material	POM C	-
Frame cavity radius	40	mm
Covering lids material	PE 1000	-
Rolling body material	steel	-
Rolling body radius	20	mm
Rolling body weight	12.8	g
Number of magnets	12	-
Magnets material	$Nd_2Fe_{14}B$ N42	-
Magnets dimensions	ø10x2	mm
Magnets weight	1.1	g
Total proof mass weight	26	g
Total proof mass moment of inertia I_{COG} (CAD)	2.48e-6	$kg.m^2$
Effective coupling coefficient (FEM)	0.20	Wb/rad
Coil wire diameter	50	µm
Coil outer radius	16	mm
Coil inner radius	6	mm
Coil height	3	mm
Coil turns	2000	-
Coil resistance	2	kΩ
Resistive load	2	kΩ
Mechanical quality factor	3.5	-

Tab. 1 *Fabricated harvester prototype data*

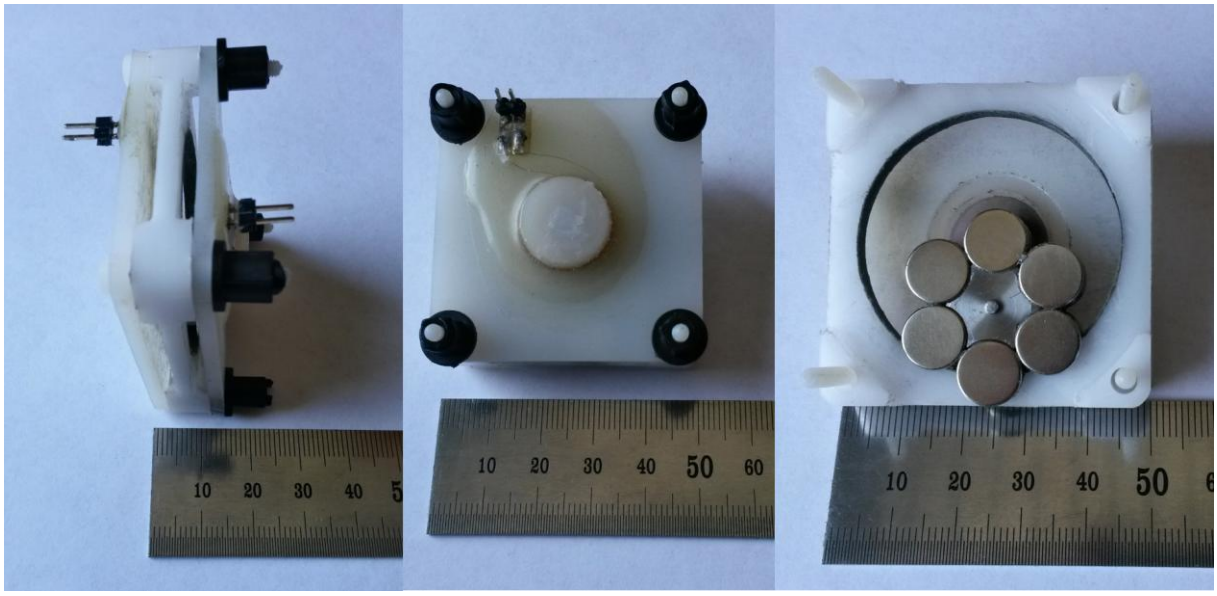

Fig. 9 *Prototype of the Tusi couple harvester*

5. Experimental Analysis

The assembled prototype was tested on a linear drive, oscillating in the horizontal plane with a range of dominant frequencies and magnitudes of acceleration. The linear drive used was not capable of delivering a harmonic excitation acceleration, thus the data presented are obtained from excitation with multiple frequency components. The acceleration data during the measurements were captured using a SlamStick C wireless datalogger containing a three axial accelerometer capable of measuring acceleration frequencies in the range of 0-500 Hz and magnitudes between ±16 g.

The voltage on a 2 kΩ resistive load was recorded for 15 measurements, each with different excitation parameters as shown in Table 2. The load was selected based on empirical results, obtained by exciting the harvester in non-controlled environment.

Measurement no.	Acceleration frequency [Hz]	Acceleration magnitude [g]	Measured RMS voltage [V]	Simulated RMS voltage [V]	Difference [V]	Difference [%]
1	2.88	0.15	**0.60**	0.66	-0.06	10.41
2	5.00	0.34	**1.04**	1.02	0.02	2.01
3	1.34	0.73	**1.05**	0.96	0.09	8.65
4	2.00	0.49	**1.09**	0.98	0.11	10.25
5	1.51	0.52	**1.23**	1.11	0.12	9.40
6	2.50	0.48	**1.33**	1.33	0.00	0.04
7	5.57	0.48	**1.38**	1.33	0.05	3.87
8	2.00	0.98	**1.65**	1.66	-0.01	0.34
9	4.16	0.45	**1.81**	1.65	0.16	8.75
10	4.16	0.65	**2.02**	2.20	-0.18	8.92
11	3.85	0.50	**2.03**	1.94	0.09	4.45
12	4.17	0.61	**2.14**	2.21	-0.07	3.24
13	3.33	0.93	**2.53**	2.71	-0.19	7.48
14	2.94	0.89	**2.63**	2.84	-0.20	7.62
15	2.78	1.30	**3.22**	3.02	0.20	6.30

Tab. 2 *Measured and simulated performance comparison*

The measured RMS voltage and power on the load exhibit a good agreement with the simulation results obtained by feeding the recorded acceleration to the model (Fig. 10), considering the manufacturing precision of the prototype and measurement uncertainties. Discrepancy over 10% between the measured and simulated performance was found only in two measurements, which is considered satisfactory.

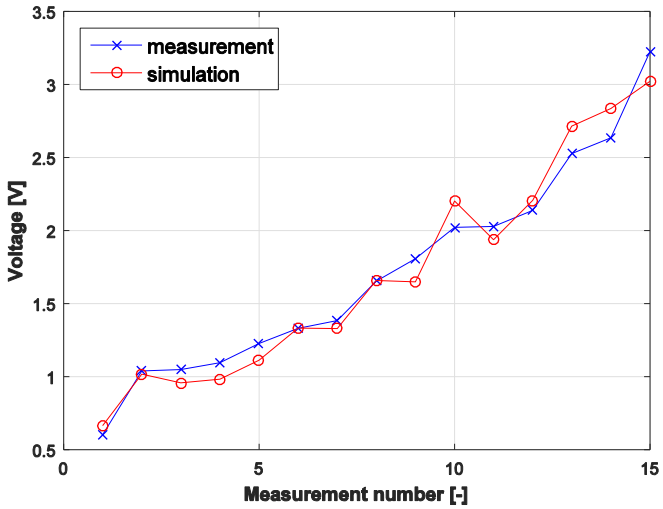

Fig. 10 *Fit of the simulation data with the experiment*

A comparison of the time domain waveforms measured and simulated also shows a good agreement between the measurement and the simulation (Fig. 11). The higher noise present on the simulated voltage waveforms is due to the numerical derivative used to model the change in total magnetic flux through the coil.

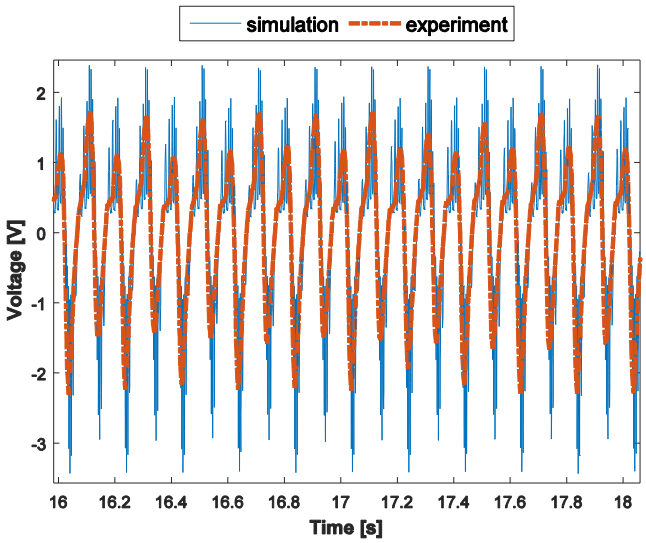

Fig. 11 *Time domain voltage waveforms simulation and experiment comparison*

The power delivered to the resistive load for the different excitation parameters is shown in Fig 12. This indicates a maximum experimentally measured power of 5.2 mW RMS, which is in excellent agreement with the simulated values.

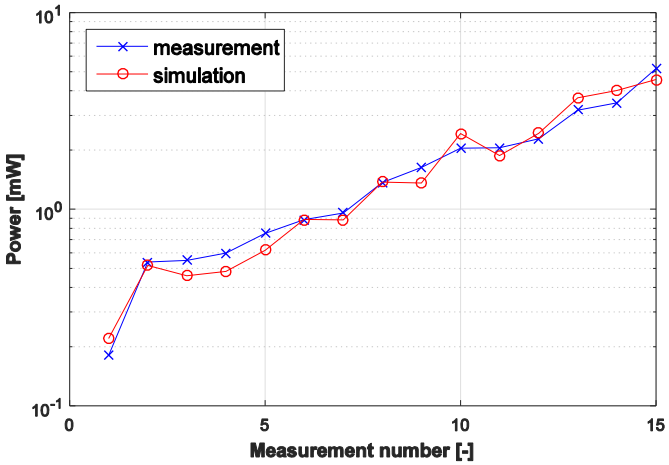

Fig. 12 *Average power on load – experiment and simulation fit*

6. Harvester performance evaluation

To enable comparison of the Tusi couple configuration harvester with other designs, normalized power density metrics [43] together with maximum power output is used. Considering the presented prototype dimensions 50x50x20 mm and the simulated voltage output on 2 kΩ resistive load, the simulated NPD of the harvester reaches values up to 230 $\mu W/g^2/cm^3$ depending on the frequency of harmonic excitation acceleration and the degree of nonlinear behaviour (Fig. 13). A comparison with other harvesters working below 10 Hz is shown in Table 3. This shows the Tusi couple design is outperforming all comparable harvesters with a single exception, which is, however, working at almost twice the frequency.

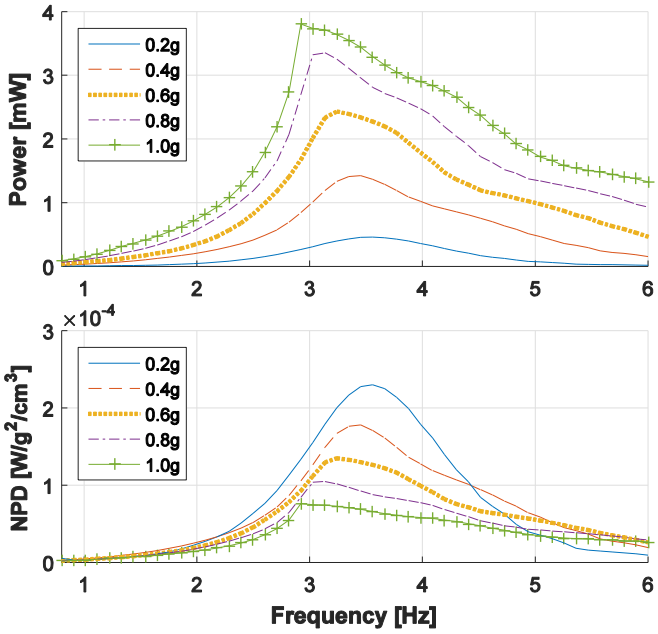

Fig. 13 Simulated performance of the harvester prototype under different harmonic excitation conditions

In this case the simulated peak NPD falls with increasing harmonic acceleration magnitude, which is due to the increasing degree of nonlinear behaviour. The NPD is not the optimal performance metric, but as it is at the moment the most widely used metric, it allows for a rough comparison of the different energy harvesters, and information necessary for calculating some other figures of merit [44]–[46] are rarely available.

Reference	Size [mm]	Frequency [Hz]	Acceleration [g]	Power output [µW]	NPD [µW/cm^3/g^2]
[47]	20x45x?	2	0.4	40	?
[48]	ø17x55	2	0.5	300	96
[49]	ø 12x80	6	0.5	4840	2140
[50]	34x34x18	8	0.5	430	83
[51]	54x46x15	9.25	0.5	550	59
This work	50x50x20	3.45	0.4	1400	178

Tab. 3 Comparison of low frequency harvesters performance

Simulated voltage and power output for different resistive loads under a constant acceleration magnitude 0.6g show a rising RMS voltage on the load with increasing resistance (Fig. 14). In terms of power output, the optimal load [52] for the harmonic excitation was found to be between 2 kΩ and 5 kΩ depending on the harmonic excitation frequency (Fig. 15).

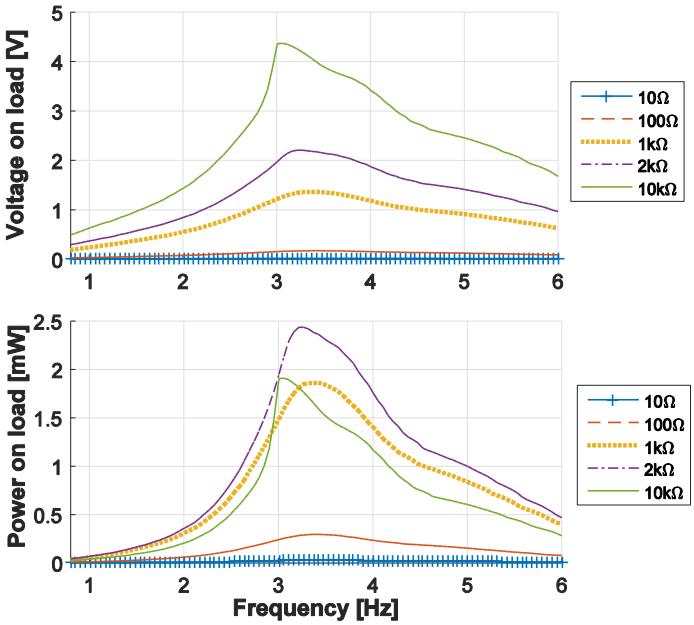

Fig. 14 Comparison of the simulated harvester performance with different resistive loads

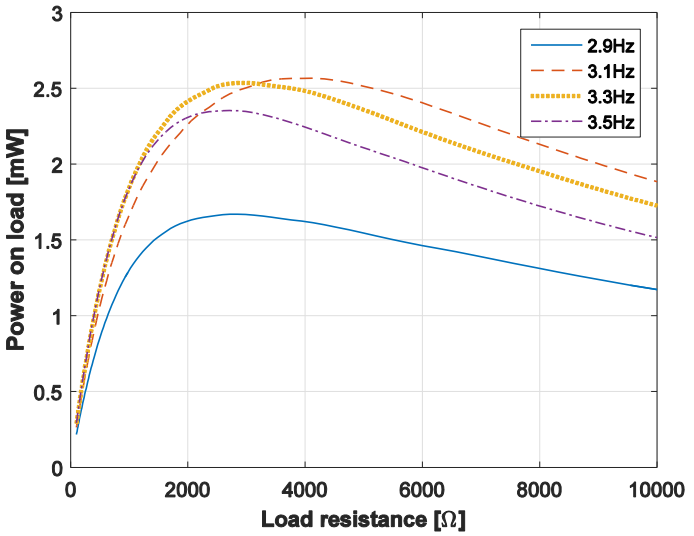

Fig. 15 Optimal resistive loads for different harmonic excitation frequencies

7. Discussion and further research directions

The simulated power outputs demonstrate the significant potential of this harvester design for use in human power energy harvesting and other very low frequency applications. Harvesters based on the Tusi couple could also present a viable alternative to current microgenerators used in wristwatches. The energy transduction method is not limited to electromagnetic induction, a similar device could be designed that uses a piezoelectric transducer that could be excited by a variable magnetic force between a magnet, fixed on the piezoelectric transducer, and the magnets on the moving proof mass. The transducing elements excitation principle would then be quite similar to the magnetically plucked [53] harvesting devices presented in [54], [55].

The main challenge of the mechanism presented lies in the precision required during assembly, which is necessary to ensure the rolling motion of the proof mass without sliding or sticking during operation.

Material selection is another crucial point, as the contact surfaces between the frame and the rolling mass need to promote the rolling motion without sliding, while the material of the covering lids with the leading slots should be selected so that lowest possible friction between the proof mass and the lids is achieved. Use of electrically

conductive materials for the frame and covering lids structures is not feasible for the presented design due to the eddy currents induction, which would increase the energy losses in the system. However, if the magnetic circuit is reworked so that the magnetic field does extend through the covering lids, the use of metals might be advantageous.

The resulting mechanical damping of the system is affected both by the assembly design and precision, and by the material selection. The future design optimization should include minimizing the mechanical damping, as this will improve the overall harvester performance.

The natural frequency of the device can be changed without changing the main dimensions by changing the weight and its distribution in the proof mass, as this will alter the generalized mass (moment of inertia). Changing the weight of the proof mass will, however, inevitably alter also the stiffness of the system. Unlike standard devices with mechanic or magnetic springs, the natural frequency cannot be changed by simply adjusting the spring stiffness. Fine tuning of the system is therefore complicated and requires redesign of at least one part to adapt the device for different working frequency range.

An asymmetric configuration of the magnets or proof mass weight distribution could be feasible in some applications. The resulting shift of the proof mass centre of gravity position away from the geometric centre of the proof mass would result in a different excitation torque from the same excitation acceleration, compared to the symmetric version. In that case, however, the motion equation becomes more complicated as it needs to account for the effects connected to the varying distance between the centre of gravity and point of contact between the proof mass and the frame.

Another possible future modification is a design with additional stationary magnets fixed on the frame. Depending on their number, orientation, and positioning, they would affect one or both of the equilibrium positions and the stiffness characteristics of the device. This approach could be beneficial especially in case where mainly vertical compound of the acceleration is to be harvested and there is no acceleration in the horizontal plane present to excite the harvester from the default equilibrium position, where it is insensitive to the excitation in the vertical direction. This modification, however, puts more practical demands on the contact between the proof mass and the frame cavity, as the magnetic forces might cause the proof mass to slide in order to align the magnetic fields of the stator and the rotor. A solution for this configuration might be in using geared contact but this would have implications on mechanical friction. It is a matter of further study, whether the increased mechanical losses caused by this would be overweighed by an increase in the harvester performance in given application.

8. Conclusions

In this paper a new design of kinetic, inertial 1DOF energy harvester for human power and other very low frequency environments is presented. The design is based on the Tusi couple, where the cylindrical proof mass rolls in a circular cavity with specified diameter ratio. This configuration allows for exploiting the acceleration inputs from multiple directions, and for an efficient design of the energy transducer itself. The proof mass follows an unrestricted full circular path, which is advantageous for low frequency oscillations, where a path of finite length would lead to either a bulky device, or energy losses due to the proof mass hitting the bumpers at the limits of the path.

A model of the device is built using the derived analytical equation of motion together with CAD and FEM modelling for the design parameters and magnetic field properties. Its performance is compared to the values, measured with the in-house fabricated prototype of the device. A theoretical performance analysis of the verified model is then presented, showing the excellent performance of the design in low frequency excitation environment.

The results of experiments conducted and simulations run on the validated model of the harvester clearly demonstrate the feasibility of the proposed energy harvester design for a low frequency environment, and its superior performance over other comparable designs both in terms of generated power, and normalized power density.

Acknowledgemets

This work is an output of research and scientific activities of NETME Centre, supported through project NETME CENTRE PLUS (LO1202) by financial means from the Ministry of Education, Youth and Sports in Czech Republic under the „National Sustainability Programme I“.

References

[1] S. M. and A. B. and I. P. and S. G. and G. P. Carman, “A broadband vibro-impacting power harvester with symmetrical piezoelectric bimorph-stops,” *Smart Mater. Struct.*, vol. 20, no. 4, p. 45013, 2011.

[2] K. V. Selvan and M. S. Mohamed Ali, “Micro-scale energy harvesting devices: Review of methodological performances in the last decade,” *Renew. Sustain. Energy Rev.*, 2016.

[3] E. Romero, R. O. Warrington, and M. R. Neuman, “Energy scavenging sources for biomedical sensors.,” *Physiol. Meas.*, vol. 30, no. 9, pp. R35-62, Sep. 2009.

[4] M. Wahbah, M. Alhawari, B. Mohammad, H. Saleh, and M. Ismail, “Characterization of Human Body-Based Thermal and Vibration Energy Harvesting for Wearable Devices,” *IEEE J. Emerg. Sel. Top. Circuits Syst.*, vol. 4, no. 3, pp. 354–363, Sep. 2014.

[5] A. Lay-Ekuakille, G. Vendramin, A. Trotta, and G. Mazzotta, “Thermoelectric generator design based on power from body heat for biomedical autonomous devices,” in *2009 IEEE International Workshop on Medical Measurements and Applications*, 2009, pp. 1–4.

[6] M.-K. Kim, M.-S. Kim, S. Lee, C. Kim, and Y.-J. Kim, “Wearable thermoelectric generator for harvesting human body heat energy,” *Smart Mater. Struct.*, vol. 23, no. 10, p. 105002, Oct. 2014.

[7] N. Gomez Estancona, A. G. Tena, J. Torca, L. Urruticoechea, L. Muniz, D. Aristimuno, J. M. Unanue, and A. Urruticoechea, “Solar recharging system for hearing aid cells,” *J Laryngol Otol*, vol. 108, no. 9, pp. 768–769, 1994.

[8] L. Xie and M. Cai, “Increased piezoelectric energy harvesting from human footstep motion by using an amplification mechanism,” *Appl. Phys. Lett.*, vol. 105, no. 14, p. 143901, Oct. 2014.

[9] S. Niu, X. Wang, F. Yi, Y. S. Zhou, and Z. L. Wang, “A universal self-charging system driven by random biomechanical energy for sustainable operation of mobile electronics,” *Nat. Commun.*, vol. 6, 2015.

[10] M. Pozzi and M. Zhu, “Plucked piezoelectric bimorphs for knee-joint energy harvesting: Modelling and experimental validation,” *Smart Mater. Struct.*, vol. 20, no. 5, 2011.

[11] A. Delnavaz and J. Voix, “Energy Harvesting for In-Ear Devices Using Ear Canal Dynamic Motion,” *IEEE Trans. Ind. Electron.*, vol. 61, no. 1, pp. 583–590, Jan. 2014.

[12] C. Dagdeviren, B. D. Yang, Y. Su, P. L. Tran, P. Joe, E. Anderson, J. Xia, V. Doraiswamy, B. Dehdashti, X. Feng, B. Lu, R. Poston, Z. Khalpey, R. Ghaffari, Y. Huang, M. J. Slepian, and J. A. Rogers, “Conformal piezoelectric energy harvesting and storage from motions of the heart, lung, and diaphragm.,” *Proc. Natl. Acad. Sci. U. S. A.*, vol. 111, no. 5, pp. 1927–32, Feb. 2014.

[13] R. Morais, N. M. Silva, P. M. Santos, C. M. Frias, J. A. F. Ferreira, A. M. Ramos, J. A. O. Simões, J. M. R. Baptista, and M. C. Reis, “Double permanent magnet vibration power generator for smart hip prosthesis,” *Sensors Actuators A Phys.*, vol. 172, no. 1, pp. 259–268, Dec. 2011.

[14] K. Remick, D. Dane Quinn, D. Michael McFarland, L. Bergman, and A. Vakakis, “High-frequency vibration energy harvesting from impulsive excitation utilizing intentional dynamic instability caused by strong nonlinearity,” *J. Sound Vib.*, vol. 370, pp. 259–279, May 2016.

[15] Z. Zhou, W. Qin, and P. Zhu, “Improve efficiency of harvesting random energy by snap-through in a quad-stable harvester,” *Sensors Actuators, A Phys.*, vol. 243, pp. 151–158, Jun. 2016.

[16] B. C. Jung, C. Cho, H. Yoon, H. Yoon, B. D. Youn, and Y. Y. Kim, “Statistical model calibration for energy harvesting skin analysis and design,” in *53rd AIAA/ASME/ASCE/AHS/ASC Structures, Structural Dynamics and Materials Conference 2012*, 2012.

[17] J. Smilek, F. Cieslar, and Z. Hadas, “Measuring acceleration in the area of human head for energy harvesting purposes,” in *Proceedings of the 2016 17th International Conference on Mechatronics - Mechatronika, ME 2016*, 2017.

[18] J. Smilek and Z. Hadas, “A study of kinetic energy harvesting for biomedical application in the head area,” *Microsyst. Technol.*, pp. 1–13, Dec. 2015.

[19] J. Yun, S. N. Patel, M. S. Reynolds, and G. D. Abowd, “Design and Performance of an Optimal Inertial Power Harvester for Human-Powered Devices,” *IEEE Trans. Mob. Comput.*, vol. 10, no. 5, pp. 669–683, May 2011.

[20] A. Cadei, A. Dionisi, E. Sardini, and M. Serpelloni, “Kinetic and thermal energy harvesters for implantable medical devices and biomedical autonomous sensors,” *Meas. Sci. Technol.*, vol. 25, no. 1, p. 12003, Jan. 2014.

[21] H. Li, C. Tian, and Z. D. Deng, “Energy harvesting from low frequency applications using piezoelectric materials,” *Applied Physics Reviews*. 2014.

[22] J. M. Kluger, T. P. Sapsis, and A. H. Slocum, “Robust energy harvesting from walking vibrations by means of nonlinear cantilever beams,” *J. Sound Vib.*, vol. 341, pp. 174–194, Apr. 2015.

[23] J. Cao, W. Wang, S. Zhou, D. J. Inman, and J. Lin, “Nonlinear time-varying potential bistable energy harvesting from human motion,” *Appl. Phys. Lett.*, vol. 107, no. 14, p. 143904, Oct. 2015.

[24] Y. N. and N. M. and K. M. and M. I. and S. Suzuki, “Electrostatic micro power generation from low-frequency vibration such as human motion,” *J. Micromechanics Microengineering*, vol. 19, no. 9, p. 94002, 2009.

[25] R. Tashiro, N. Kabei, K. Katayama, F. Tsuboi, and K. Tsuchiya, “Development of an electrostatic generator for a cardiac pacemaker that harnesses the ventricular wall motion,” *J. Artif. Organs*, vol. 5, no. 4, 2002.

[26] Y. Zi, H. Guo, Z. Wen, M.-H. Yeh, C. Hu, and Z. L. Wang, “Harvesting Low-Frequency (<5 Hz) Irregular Mechanical Energy: A Possible Killer Application of Triboelectric Nanogenerator,” *ACS Nano*, vol. 10, no. 4, 2016.

[27] S. D. Moss, O. R. Payne, G. A. Hart, and C. Ung, “Scaling and power density metrics of electromagnetic vibration energy harvesting devices,” *Smart Mater. Struct.*, vol. 24, no. 2, 2015.

[28] W. Yang and S. Towfighian, “A hybrid nonlinear vibration energy harvester,” *Mech. Syst. Signal Process.*, 2017.

[29] Ö. Zorlu, E. T. Topal, and H. Külah, “A vibration-based electromagnetic energy harvester using mechanical frequency up-conversion method,” *IEEE Sens. J.*, vol. 11, no. 2, 2011.

[30] M. Scapolan, M. G. Tehrani, and E. Bonisoli, “Energy harvesting using parametric resonant system due to time-varying damping,” *Mech. Syst. Signal Process.*, 2016.

[31] Y. Z. and C. S. C. and B. Kong, “A low frequency nonlinear energy harvester with large bandwidth utilizing magnet levitation,” *Smart Mater. Struct.*, vol. 24, no. 4, p. 45019, 2015.

[32] A. Haroun, I. Yamada, and S. Warisawa, “Study of electromagnetic vibration energy harvesting with free/impact motion for low frequency operation,” *J. Sound Vib.*, 2015.

[33] A. Haroun, I. Yamada, and S. Warisawa, “Micro electromagnetic vibration energy harvester based on free/impact motion for low frequency-large amplitude operation,” *Sensors Actuators, A Phys.*, vol. 224, pp. 87–98, Apr. 2015.

[34] S.-J. Jang, I.-H. Kim, H.-J. Jung, and Y.-P. Lee, “A tunable rotational energy harvester for low frequency vibration,” *Appl. Phys. Lett.*, vol. 99, no. 13, p. 134102, 2011.

[35] B. J. Bowers and D. P. Arnold, “Spherical, rolling magnet generators for passive energy harvesting from human motion,” *J. Micromechanics Microengineering*, vol. 19, no. 9, p. 94008, Sep. 2009.

[36] F. K. Shaikh and S. Zeadally, “Energy harvesting in wireless sensor networks: A comprehensive review,” *Renewable and Sustainable Energy Reviews*. 2016.

[37] A. R. M. Siddique, S. Mahmud, and B. Van Heyst, “A comprehensive review on vibration based micro power generators using electromagnetic and piezoelectric transducer mechanisms,” *Energy Conversion and Management*. 2015.

[38] C. Wei and X. Jing, “A comprehensive review on vibration energy harvesting: Modelling and realization,” *Renew. Sustain. Energy Rev.*, vol. 74, pp. 1–18, 2017.

[39] C. Cepnik, R. Lausecker, and U. Wallrabe, “Review on Electrodynamic Energy Harvesters—A Classification Approach,” *Micromachines*, vol. 4, no. 2, pp. 168–196, Apr. 2013.

[40] D. Spreemann, Y. Manoli, B. Folkmer, and D. Mintenbeck, “Non-resonant vibration conversion,” *J. Micromechanics Microengineering*, vol. 16, no. 9, pp. S169–S173, Sep. 2006.

[41] K. Sasaki, Y. Osaki, J. Okazaki, H. Hosaka, and K. Itao, “Vibration-based automatic power-generation system,” *Microsyst. Technol.*, vol. 11, no. 8, pp. 965–969, 2005.

[42] Z. Hadas, V. Vetiska, R. Huzlik, and V. Singule, “Model-based design and test of vibration energy harvester for aircraft application,” *Microsyst. Technol.*, vol. 20, no. 4–5, pp. 831–843, Jan. 2014.

[43] S. P. Beeby, R. N. Torah, M. J. Tudor, P. Glynne-Jones, T. O’Donnell, C. R. Saha, and S. Roy, “A micro electromagnetic generator for vibration energy harvesting,” *J. Micromechanics Microengineering*, vol. 17, no. 7, 2007.

[44] D. Mallick, A. Amann, and S. Roy, “Interplay between electrical and mechanical domains in a high performance nonlinear energy harvester,” *Smart Mater. Struct.*, vol. 24, no. 12, p. 122001, 2015.

[45] G. Sebald, H. Kuwano, D. Guyomar, and B. Ducharne, “Experimental Duffing oscillator for broadband piezoelectric energy harvesting,” *Smart Mater. Struct.*, vol. 20, no. 10, p. 102001, 2011.

[46] P. D. Mitcheson, E. M. Yeatman, G. K. Rao, A. S. Holmes, and T. C. Green, “Energy Harvesting From Human and Machine Motion for Wireless Electronic Devices,” *Proc. IEEE*, vol. 96, no. 9, pp. 1457–1486, Sep. 2008.

[47] Y. Naruse, N. Matsubara, K. Mabuchi, M. Izumi, and S. Suzuki, “Electrostatic micro power generation from low-frequency vibration such as human motion,” *J. Micromechanics Microengineering*, vol. 19, no. 9, p. 94002, Sep. 2009.

[48] C. R. Saha, T. O'Donnell, N. Wang, and P. McCloskey, “Electromagnetic generator for harvesting energy from human motion,” *Sensors Actuators, A Phys.*, vol. 147, no. 1, pp. 248–253, Sep. 2008.

[49] A. Munaz, B.-C. Lee, and G.-S. Chung, “A study of an electromagnetic energy harvester using multi-pole magnet,” *Sensors Actuators A Phys.*, vol. 201, pp. 134–140, Oct. 2013.

[50] S. E. Jo, M. S. Kim, and Y. J. Kim, “Electromagnetic human vibration energy harvester comprising planar coils,” *Electron. Lett.*, vol. 48, no. 14, p. 874, 2012.

[51] S. C. and D. P. Arnold, “A study of a multi-pole magnetic generator for low-frequency vibrational energy harvesting,” *J. Micromechanics Microengineering*, vol. 20, no. 2, p. 25015, 2010.

[52] A. Cammarano, S. A. Neild, S. G. Burrow, D. J. Wagg, and D. J. Inman, “Optimum resistive loads for vibration-based electromagnetic energy harvesters with a stiffening nonlinearity,” *J. Intell. Mater. Syst. Struct.*, 2014.

[53] T. Xue and S. Roundy, “On magnetic plucking configurations for frequency up-converting mechanical energy harvesters,” *Sensors Actuators, A Phys.*, 2017.

[54] K. Fan, J. Chang, F. Chao, and W. Pedrycz, “Design and development of a multipurpose piezoelectric energy harvester,” *Energy Convers. Manag.*, vol. 96, pp. 430–439, May 2015.

[55] P. Pillatsch, E. M. Yeatman, and A. S. Holmes, “A piezoelectric frequency up-converting energy harvester with rotating proof mass for human body applications,” *Sensors Actuators, A Phys.*, 2014.

Table 1

Parameter	Value	Unit
Total dimensions	50x50x20	mm
Total weight	56.3	g
Frame material	POM C	-
Frame cavity radius	40	mm
Covering lids material	PE 1000	-
Rolling body material	steel	-
Rolling body radius	20	mm
Rolling body weight	12.8	g
Number of magnets	12	-
Magnets material	$Nd_2Fe_{14}B$ N42	-
Magnets dimensions	ø10x2	mm
Magnets weight	1.1	g
Total proof mass weight	26	g
Total proof mass moment of inertia I_{COG} (CAD)	2.48E-06	$kg.m^2$
Effective coupling coefficient (FEM)	0.2	Wb/rad
Coil wire diameter	50	µm
Coil outer radius	16	mm
Coil inner radius	6	mm
Coil height	3	mm
Coil turns	2000	-
Coil resistance	2	kΩ
Resistive load	2	kΩ
Mechanical quality factor	3.5	-

Table 2

Measurement no.	Acceleration frequency [Hz]	Acceleration magnitude [g]	Measured RMS voltage [V]	Simulated RMS voltage [V]	Difference [V]	Difference [%]
1	2.88	0.15	**0.6**	0.66	-0.06	10.41
2	5	0.34	**1.04**	1.02	0.02	2.01
3	1.34	0.73	**1.05**	0.96	0.09	8.65
4	2	0.49	**1.09**	0.98	0.11	10.25
5	1.51	0.52	**1.23**	1.11	0.12	9.4
6	2.5	0.48	**1.33**	1.33	0	0.04
7	5.57	0.48	**1.38**	1.33	0.05	3.87
8	2	0.98	**1.65**	1.66	-0.01	0.34
9	4.16	0.45	**1.81**	1.65	0.16	8.75
10	4.16	0.65	**2.02**	2.2	-0.18	8.92
11	3.85	0.5	**2.03**	1.94	0.09	4.45
12	4.17	0.61	**2.14**	2.21	-0.07	3.24
13	3.33	0.93	**2.53**	2.71	-0.19	7.48
14	2.94	0.89	**2.63**	2.84	-0.2	7.62
15	2.78	1.3	**3.22**	3.02	0.2	6.3

Table 3

Reference	Size [mm]	Frequency [Hz]	Acceleration [g]	Power output [µW]	NPD [$\mu W/cm^3/g^2$]
[47]	20x45x?	2	0.4	40	?
[48]	ø17x55	2	0.5	300	96
[49]	ø 12x80	6	0.5	4840	2140
[50]	34x34x18	8	0.5	430	83
[51]	54x46x15	9.25	0.5	550	59
This work	50x50x20	3.45	0.4	1400	178

Figure 1

Click here to download high resolution image

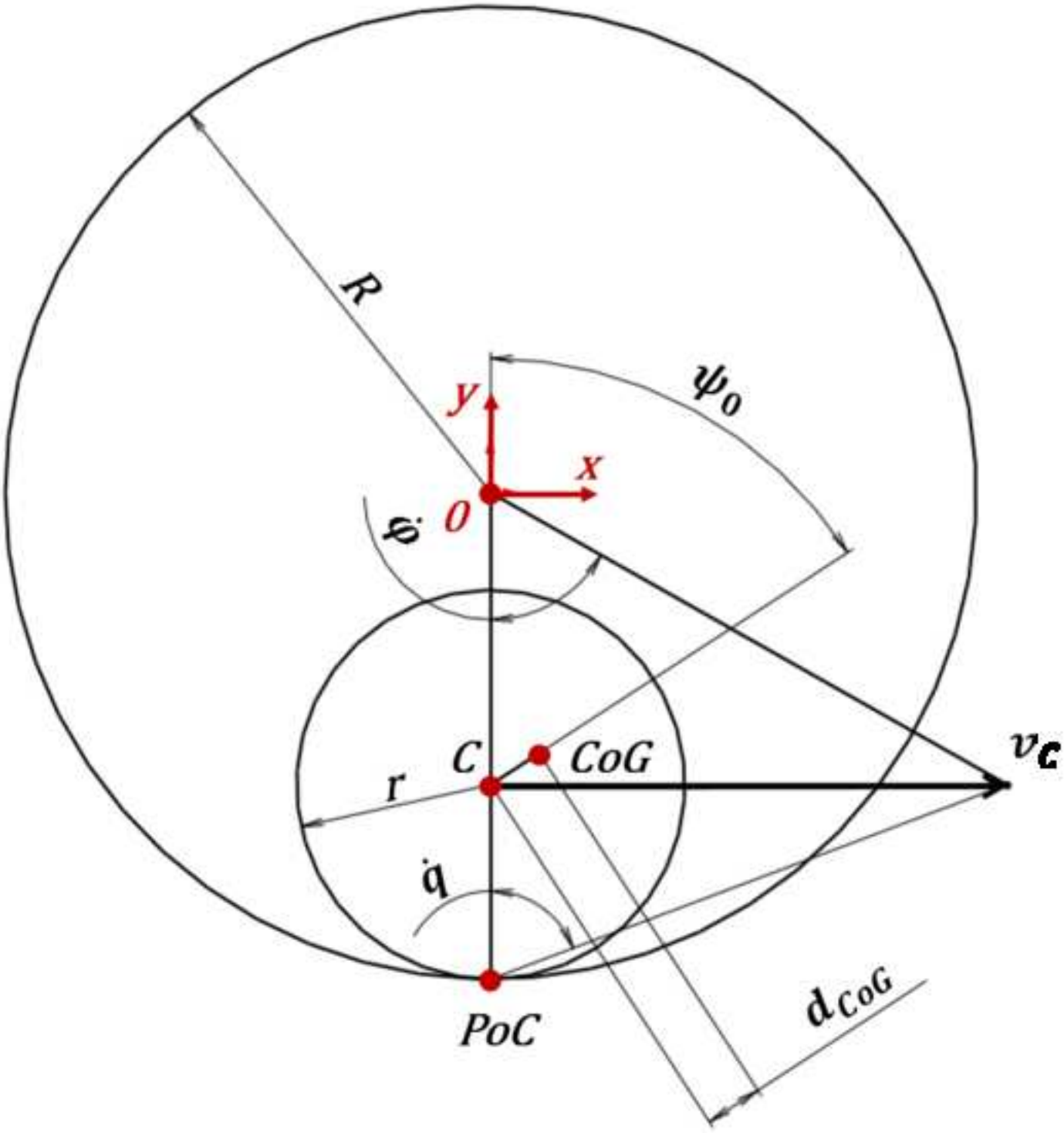

Figure 2

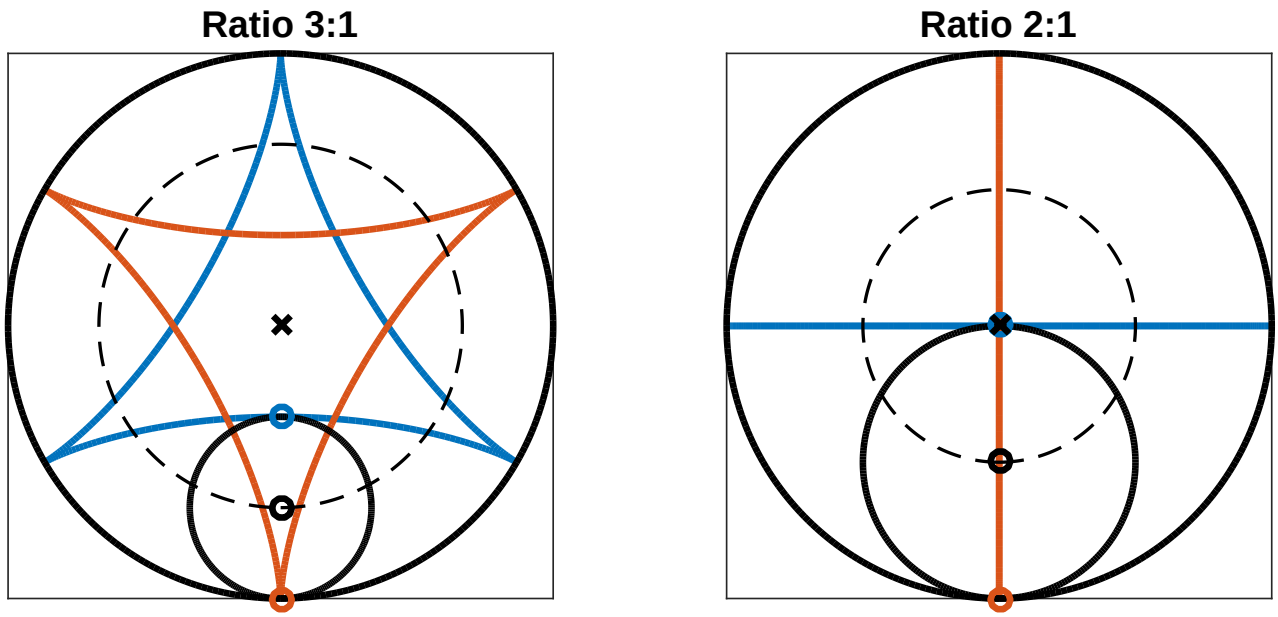

Figure 3

Click here to download high resolution image

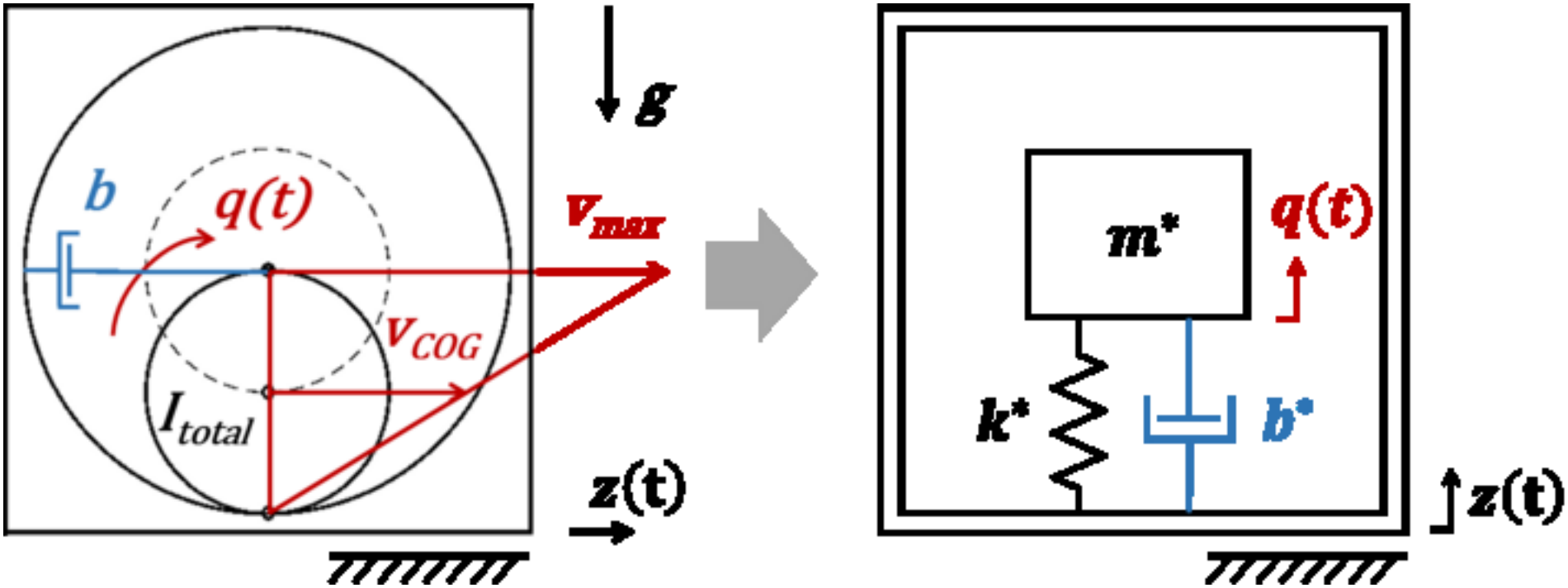

Figure 4

Click here to download high resolution image

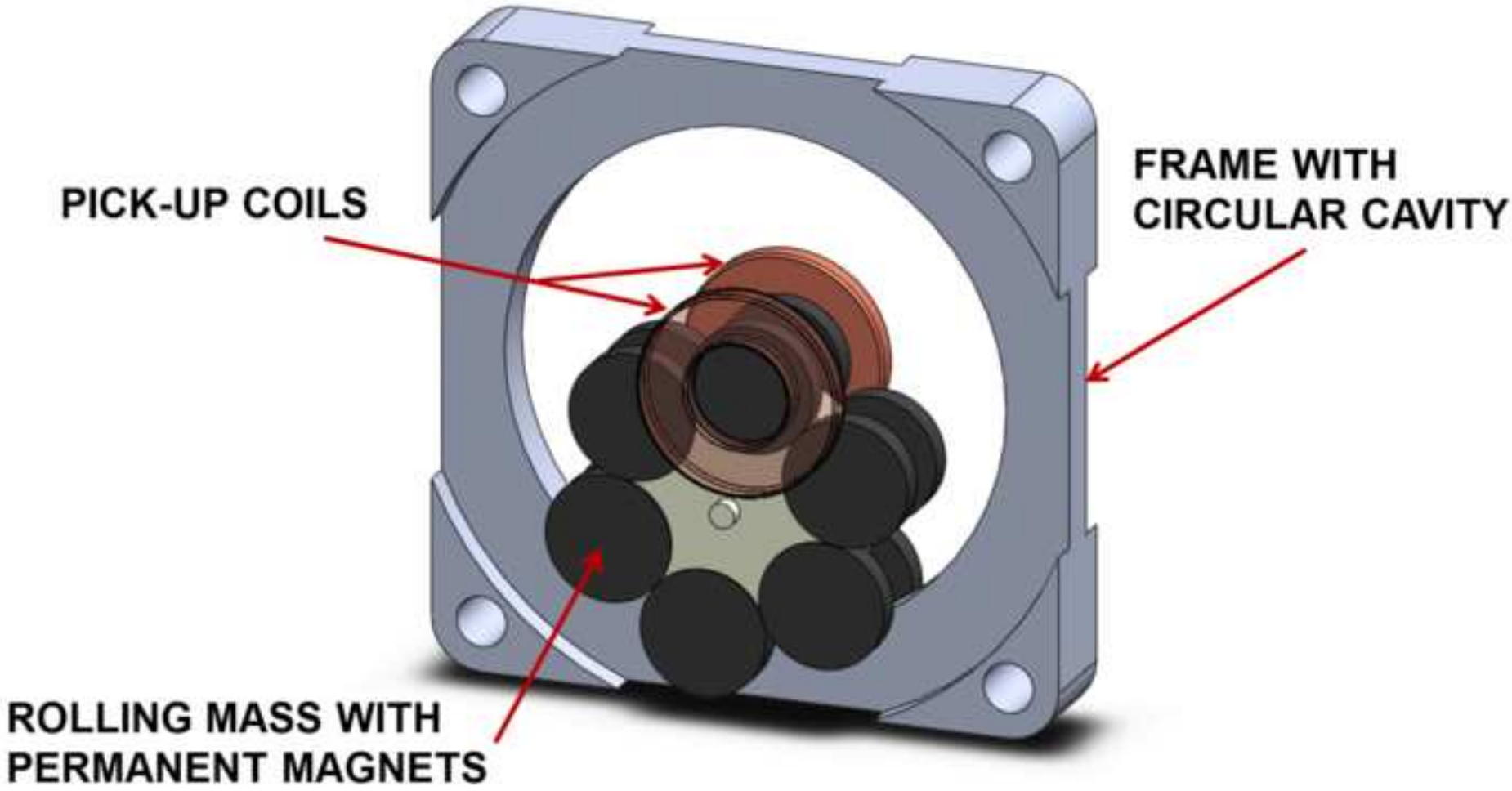

Figure 5

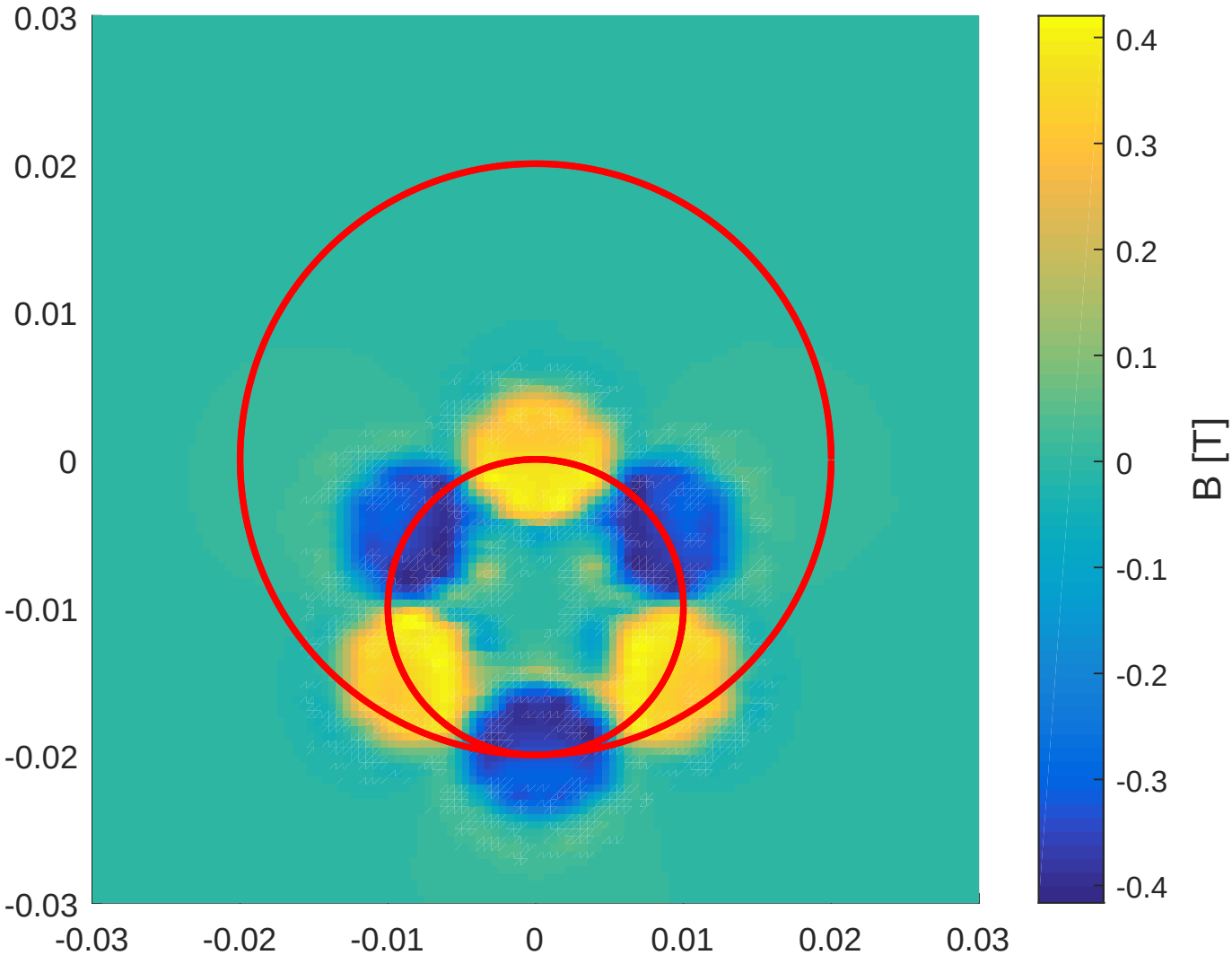
0.03
0.02
0.01
0
-0.01
-0.02
-0.03
-0.03
-0.02
-0.01
0
0.01
0.02
0.03
0.4
0.3
0.2
0.1
0
-0.1
-0.2
-0.3
-0.4
B [T]

Figure 6

Click here to download high resolution image

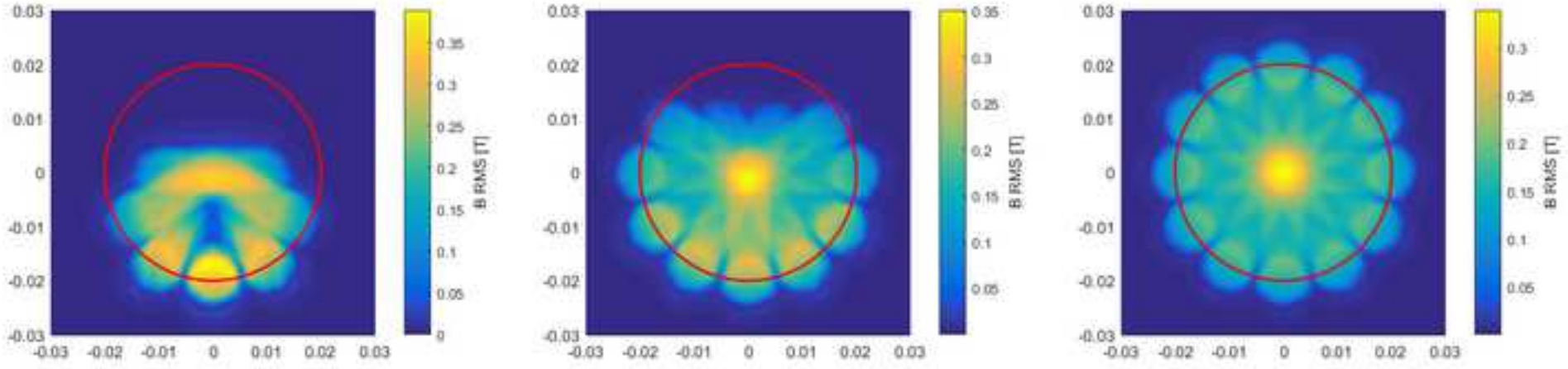

Figure 7

Click here to download high resolution image

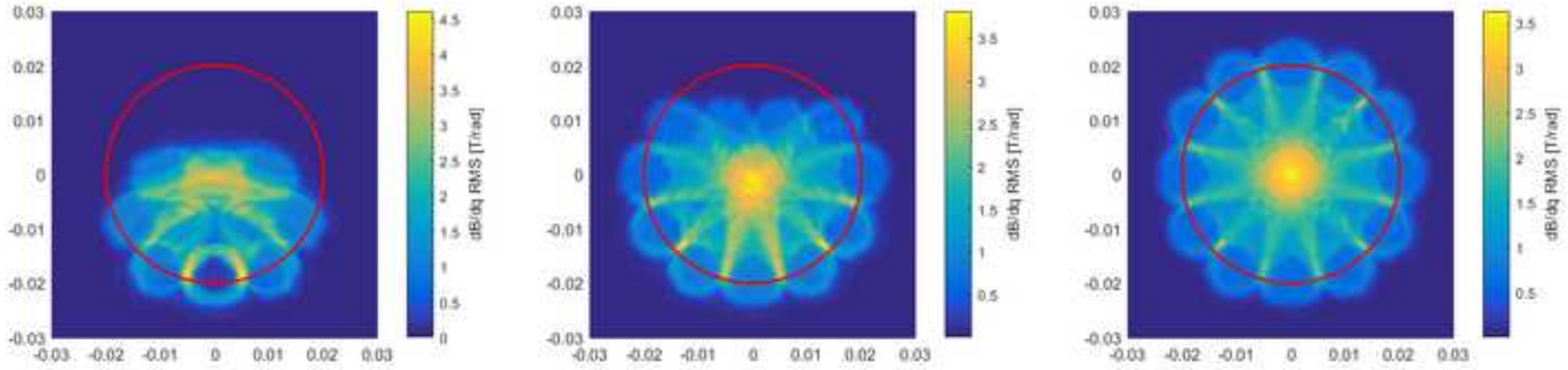

Figure 8

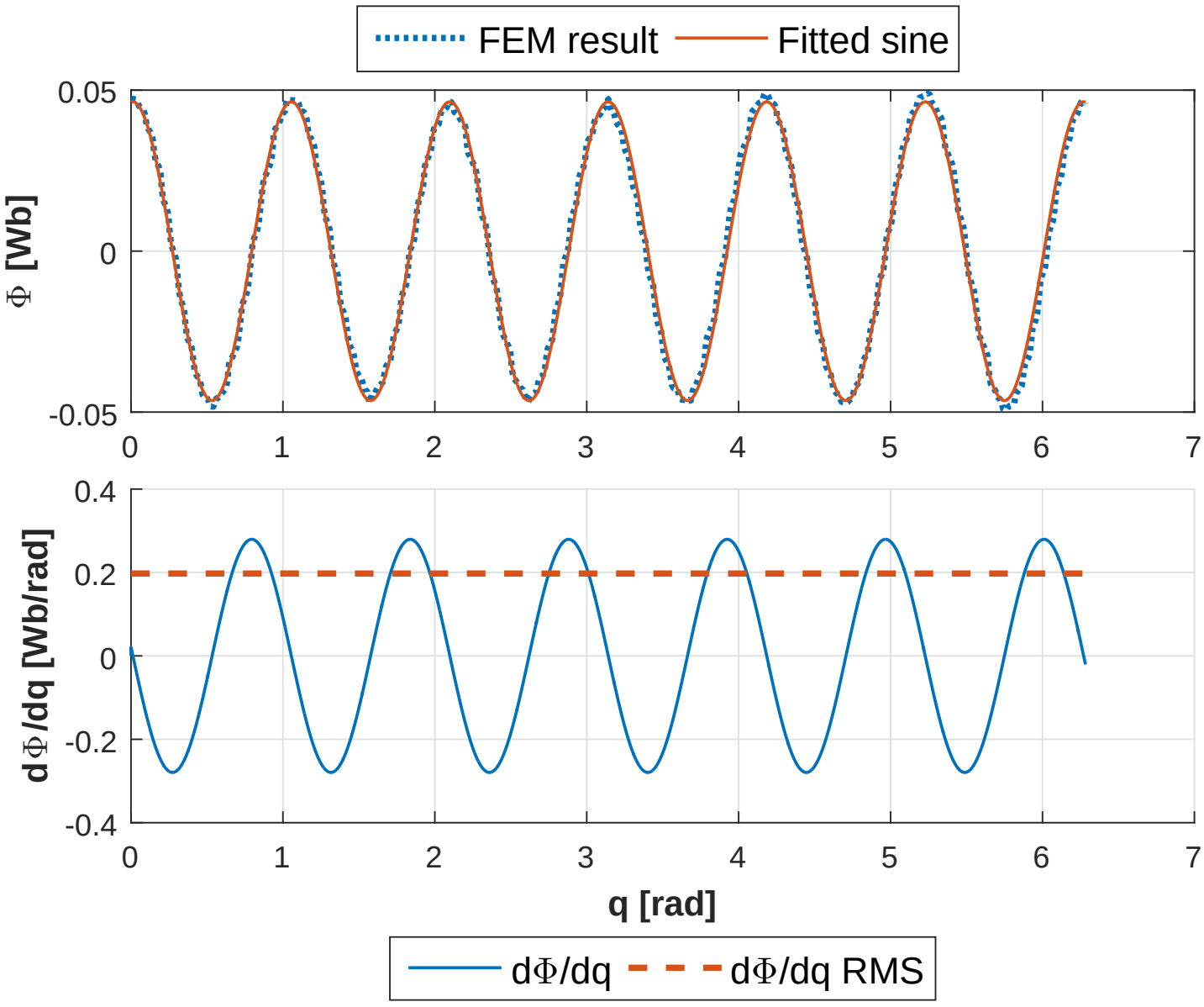
FEM result
Fitted sine
0.05
0
-0.05
Φ [Wb]
0
1
2
3
4
5
6
7
0.4
0.2
0
-0.2
-0.4
dΦ/dq [Wb/rad]
q [rad]
dΦ/dq
dΦ/dq RMS

Figure 9

Click here to download high resolution image

Figure 10

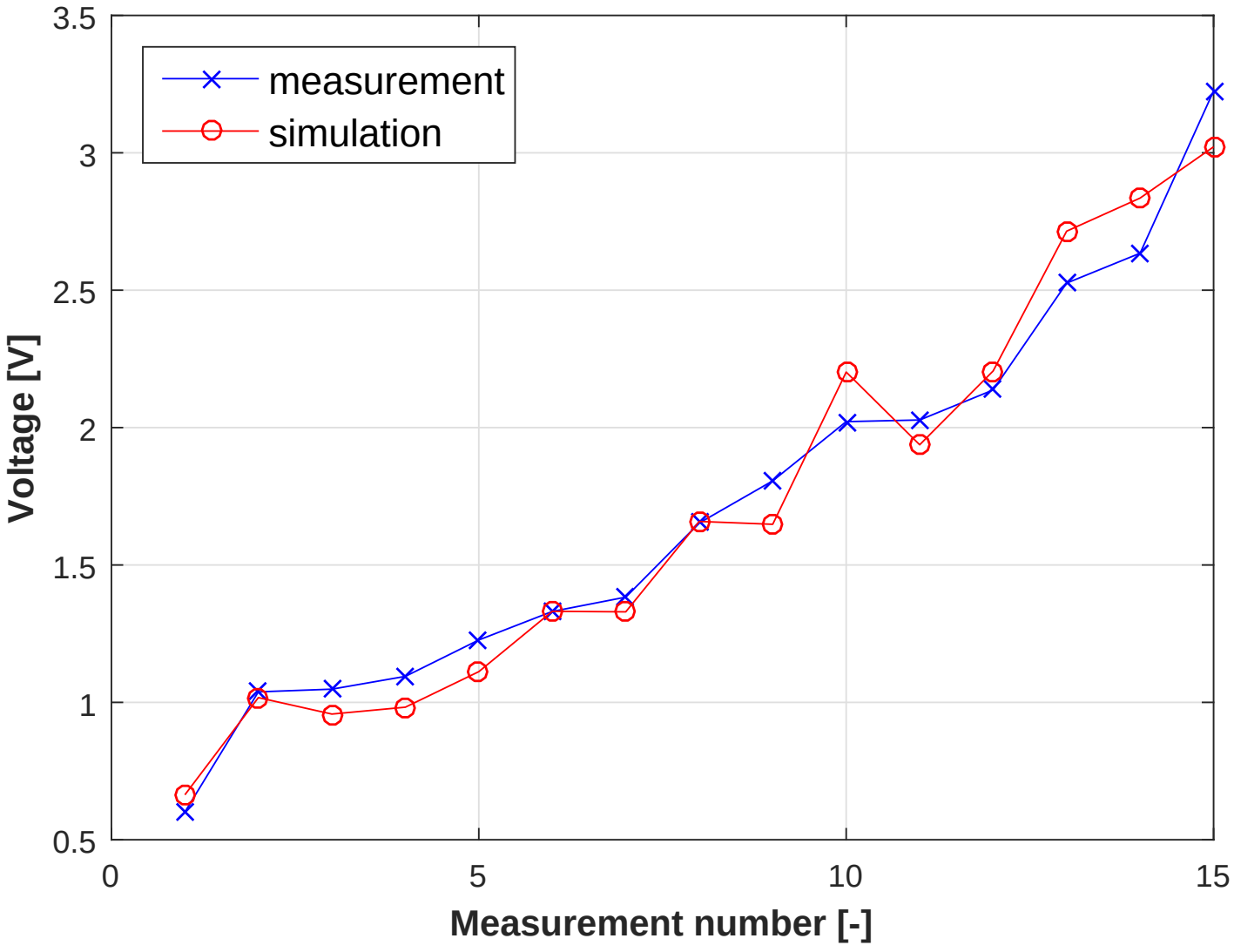
measurement
simulation
Voltage [V]
Measurement number [-]
3.5
3
2.5
2
1.5
1
0.5
0
5
10
15

Figure 11

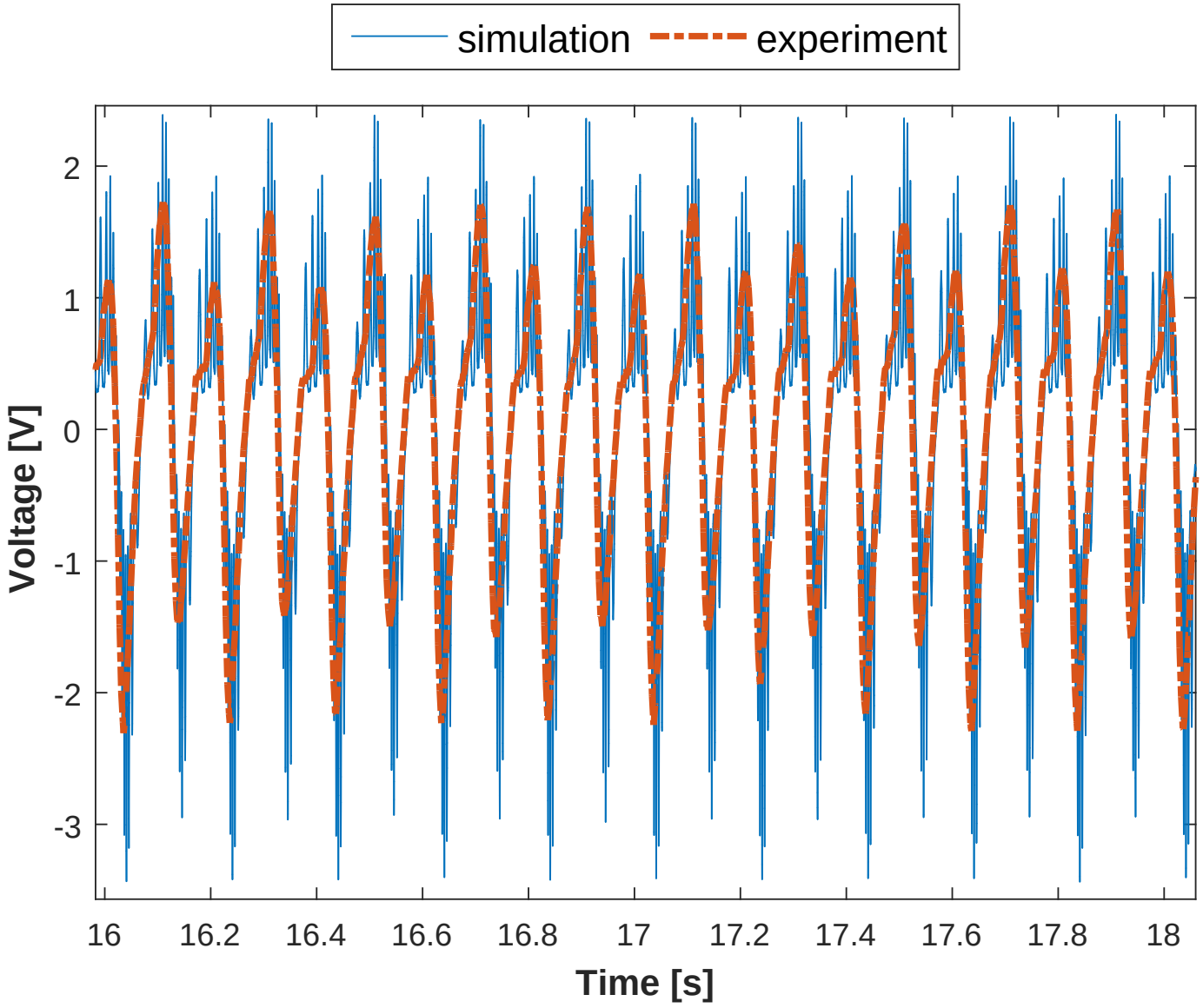
simulation
experiment
Voltage [V]
2
1
0
-1
-2
-3
16
16.2
16.4
16.6
16.8
17
17.2
17.4
17.6
17.8
18
Time [s]

Figure 12

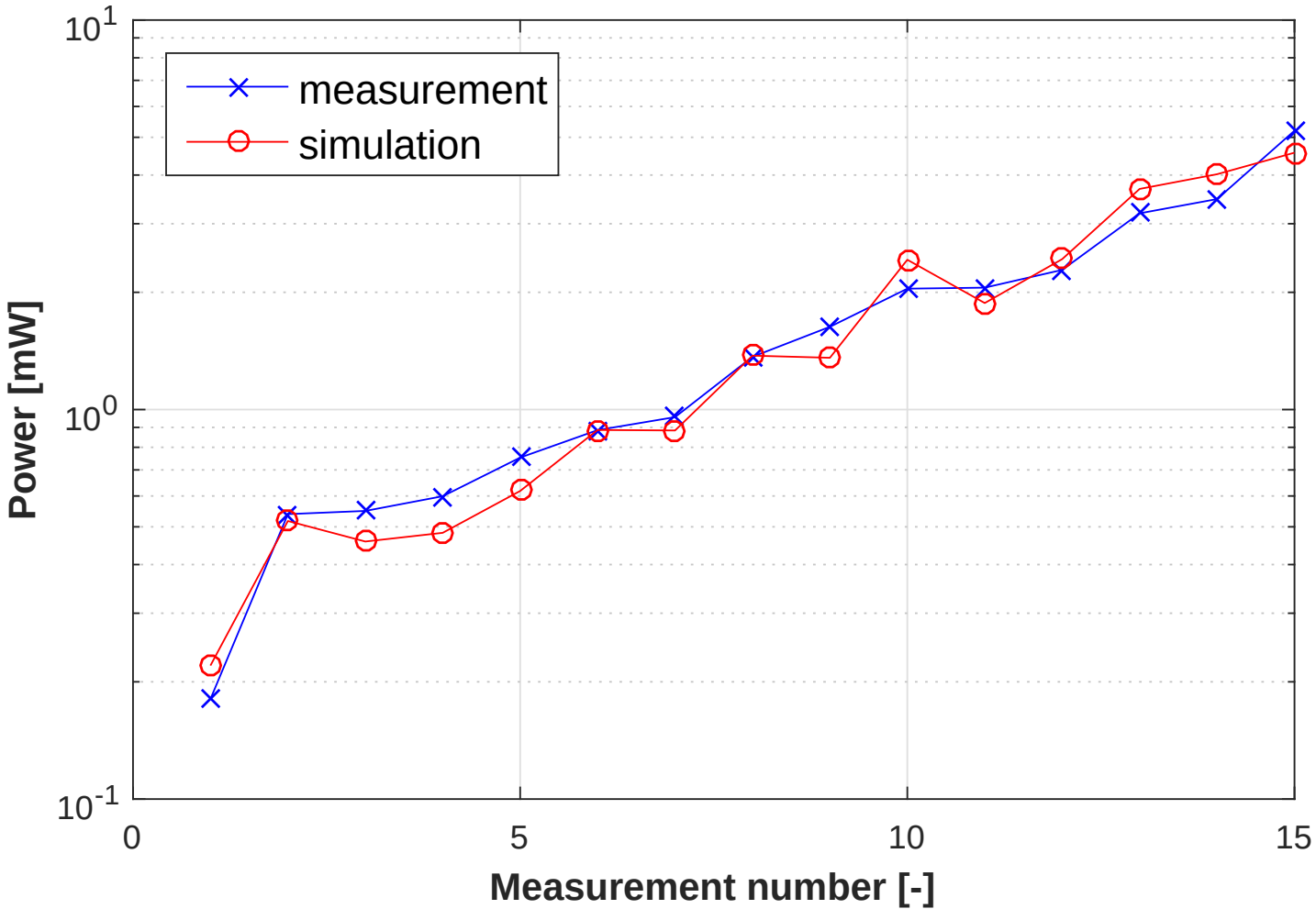
measurement
simulation
10^1
10^0
10^{-1}
Power [mW]
0
5
10
15
Measurement number [-]

Figure 13

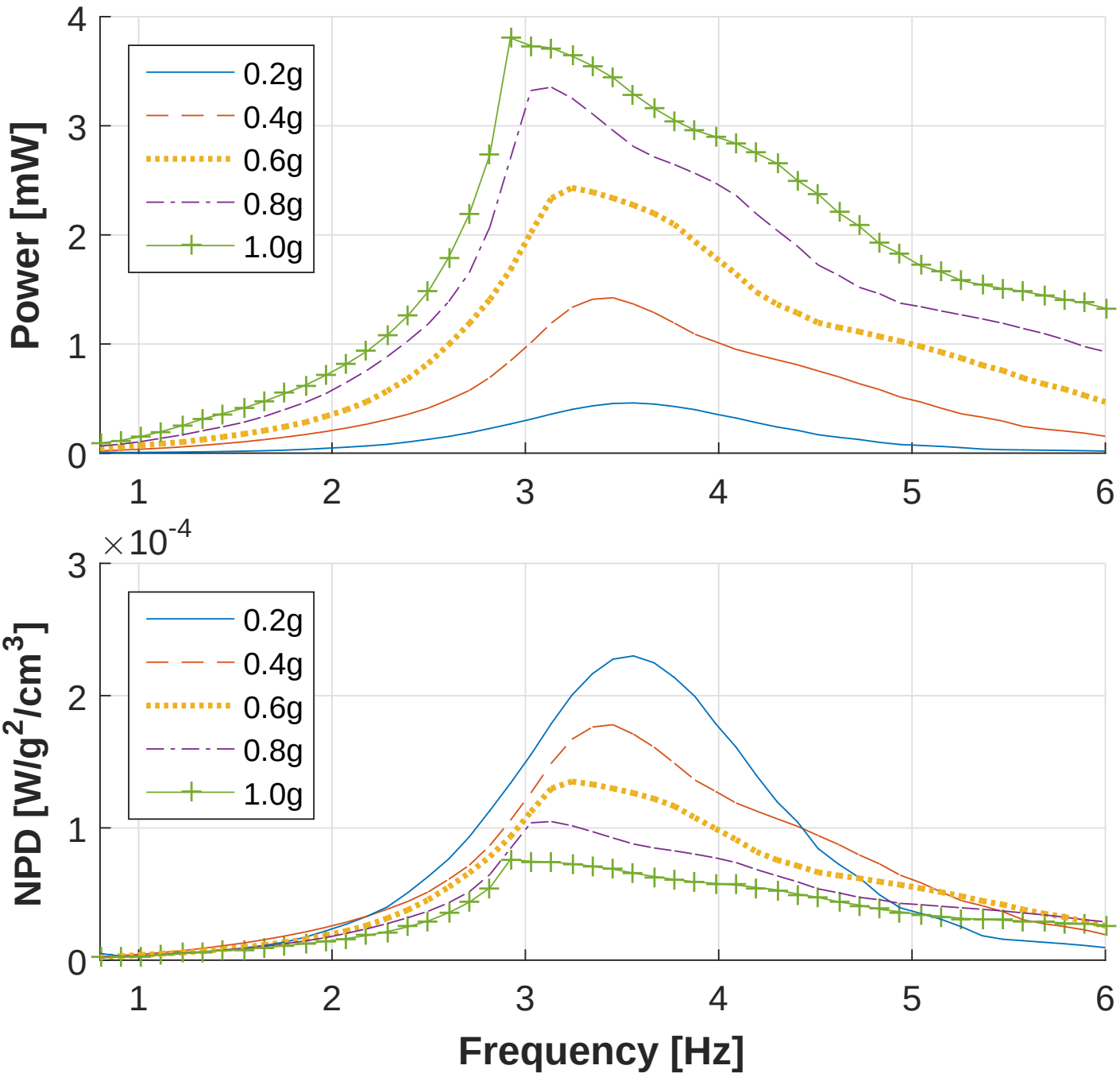
Power [mW]
0.2g
0.4g
0.6g
0.8g
1.0g
0
1
2
3
4
1
2
3
4
5
6
×10-4
NPD [W/g2/cm3]
0
1
2
3
Frequency [Hz]

Figure 14

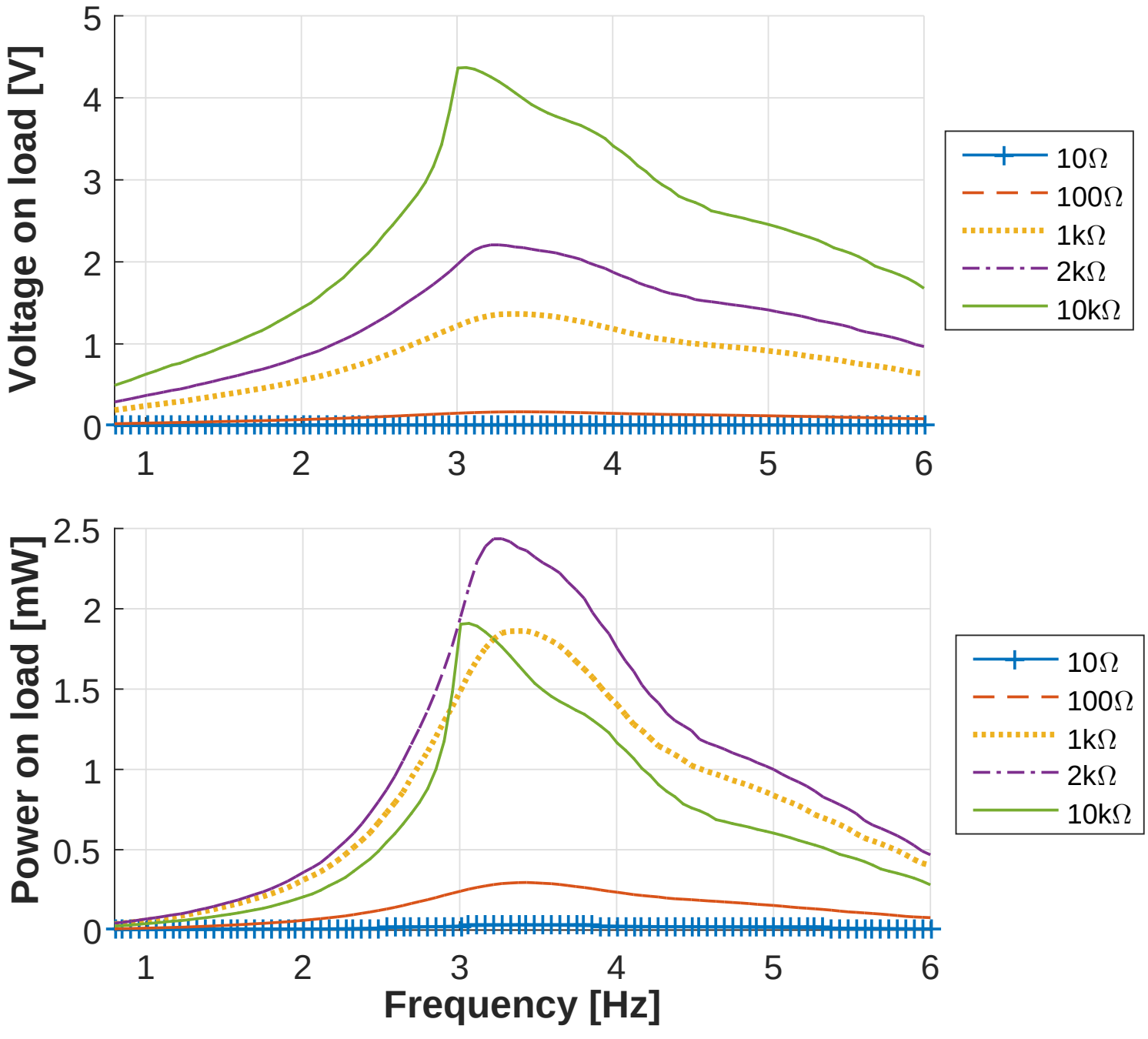
Voltage on load [V]
0
1
2
3
4
5
1
2
3
4
5
6
10Ω
100Ω
1kΩ
2kΩ
10kΩ
Power on load [mW]
0
0.5
1
1.5
2
2.5
1
2
3
4
5
6
Frequency [Hz]
10Ω
100Ω
1kΩ
2kΩ
10kΩ

Figure 15

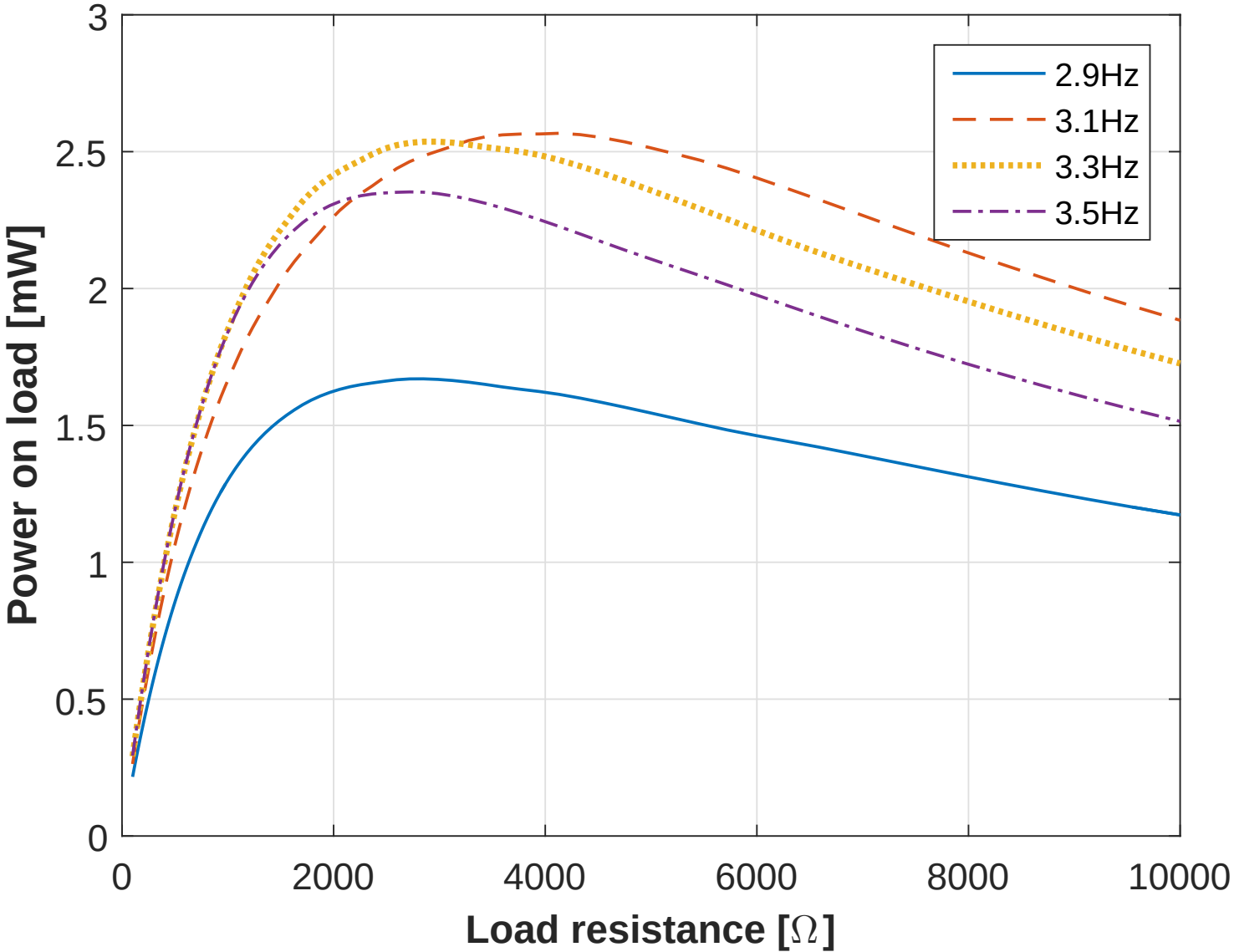
Power on load [mW]
Load resistance [Ω]
0
0.5
1
1.5
2
2.5
3
0
2000
4000
6000
8000
10000
2.9Hz
3.1Hz
3.3Hz
3.5Hz